

Primitive Quantum Gates for an $SU(3)$ Discrete Subgroup: $\Sigma(72 \times 3)$

Sebastian Osorio Perez ^{1,2,*} Edison M. Murairi ^{1,3,†} Erik J. Gustafson ^{4,‡} and Henry Lamm ^{1,3,§}

¹*Fermi National Accelerator Laboratory, Batavia, IL 60510, USA*

²*Department of Physics, University of Maryland, College Park, MD 20742, USA*

³*Superconducting and Quantum Materials System Center (SQMS), Batavia, IL, 60510, USA.*

⁴*Universities Space Research Association, Research Institute for Advanced Computer Science (RIACS) at NASA Ames Research Center, Moffett Field, California, 94035, USA*

We construct a primitive gate set for the digital quantum simulation of a discrete subgroup of $SU(3)$: the 216-element $\Sigma(72 \times 3)$. The necessary primitives are the inversion gate, the group multiplication gate, the trace gate, and the group Fourier transform, for which we provide qubit decompositions. The resulting fault-tolerant T gate costs for a fiducial calculation of shear viscosity would require about 10^{12} T gates which compares favorably to other modern estimates.

I. INTRODUCTION

While classical computers have demonstrated great success in computing properties of gauge theories with Monte Carlo methods, this approach fails for real time dynamics of the system or at finite fermion density due to the sign problems [1–4]. Quantum computers can study these problems but the limited quantum resources require efficient implementations of the infinite-dimensional bosonic degrees of freedom and their interactions.

To this end, several bosonic digitizations have been proposed in the past decade. Some quantize in the representation (electric field) basis, and impose a cut off on the maximal representation [5–26] while the q -deformed formulation [27, 28] replaces the gauge group by a quantum group. Other digitizations reformulate the degrees of freedom, for example: loop-string-hadron formulation [29–33], light-front quantization [34–36], conformal truncation [37], strong-coupling and large- N_c expansions [38, 39], fuzzy gauge theories from non-commutative geometry [40], and quantum link models [41–51]. Across this breadth, the typical estimate for qubits per local degree of freedom is $\mathcal{O}(10)$ for reasonable approximations of $SU(3)$, but establishing their connections to the continuum quantum field theory is non-trivial [40, 42, 52]. Most approaches considered only qubit methods, but there has been an increasing interest in qudits [11, 21, 28, 53–59].

In this work, we continue the study of the discrete subgroup approximation [29, 57, 60–75] which has its roots in the classical Euclidean lattice field theory [61, 62, 64, 76–85]. The discrete subgroup approximation has several advantages. First, it provides a mapping to integers while preserving a remnant of gauge symmetry; replacing fixed- or floating-point arithmetic with modular arithmetic. The discrete symmetry also allows for coupling the gauge redundancy to quantum error correction schemes [72, 86–89]. Third, the quantum memory requirements are fixed for a

TABLE I. Parameters of a crystal-like subgroups of $SU(3)$. ΔS is the gap between $\mathbb{1}$ and the nearest neighbors to it. \mathcal{N} is number of group elements that neighbor the $\mathbb{1}$.

G	ΔS	\mathcal{N}	β_f^{2+1d}	β_f^{3+1d}
$\Sigma(36 \times 3)$	$\frac{2}{3}$	18	3.78(2)	2.52(3)
$\Sigma(72 \times 3)$	$\frac{2}{3}$	54	4.223(1)	3.18(3)

given discrete subgroup and improvement in truncation error require only including additional interactions and thus circuit depth [82, 90]. This contrasts with other digitizations where reducing error requires more memory and deeper circuits. Finally, discrete subgroup approximations can be studied classically [82, 91]; something other digitizations can struggle with due to sign problems.

On the other hand, the discrete subgroup approximation requires trade offs. For nonabelian theories, one is limited to the small number of *crystal-like* subgroups with the correct center. For $SU(3)$ there are only four choices: $\Sigma(\phi \times 3)$ for $\phi = 36, 72, 216, 360$. On the lattice, there are first-order phase transitions at some *freezeout* coupling β_f (or lattice spacing a_f) that separates the discrete group from the continuum limit of the continuous group. These β_f , alongside other important properties of the smallest crystal-like subgroups of $SU(3)$ discrete groups are found in Tab. I. We agree with previous work on these groups [78], but report higher precision values. Theoretical work has shown that in the continuum the field theory of discrete groups is related to the symmetry-broken phase of continuous groups coupled to Higgs bosons in particular representations [92–96]. Recent work has begun to quantify this connection for non-abelian groups [91].

In this work, we consider the crystal-like subgroup of a $SU(3) - \Sigma(72 \times 3)$ which has 216 elements. Dependence of the lattice energy on coupling in the Wilson action are shown in Fig. 1. The elements of $\Sigma(72 \times 3)$ can be encoded into a register consisting of 9 qubits. This work constitutes another rung in the ladder of discrete subgroups for quantum simulation following previous work on smaller groups. Subgroups of $SU(2)$ studied are: the $2N$ -element dihedral groups D_N [60, 97–99], the 8-element

* sebasop@umd.edu

† emurairi@fnal.gov

‡ egustafson@usra.edu

§ hlamm@fnal.gov

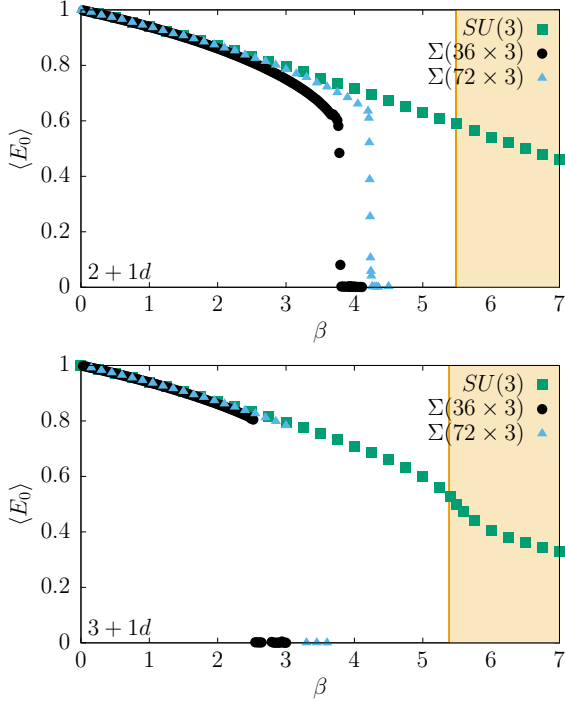


FIG. 1. Euclidean calculations of the expectation value of the plaquette $\langle E_0 \rangle$ as a function of Wilson coupling β on 8^d lattices for (top) $(2+1)$ -dimensions (bottom) $(3+1)$ -dimensions. The shaded region indicates the scaling regime $\beta \geq \beta_s$.

\mathbb{Q}_8 [57], the 24-element \mathbb{BT} [100], the 48 element \mathbb{BO} [101], the 120 element \mathbb{B} [102]. For $SU(3)$, primitive gates have only been derived for the 108-element $\Sigma(36 \times 3)$ [103].

From Fig. 1, we see that freeze-out occurs before the scaling regime. This implies that the Kogut-Susskind Hamiltonian would be insufficient for $\Sigma(72 \times 3)$ to approximate the continuum limit of $SU(3)$ and including additional interactions is necessary [62, 64, 81, 82, 91]. Together with arguments relating lattice actions to lattice Hamiltonians [66, 83, 104–106], this suggests that discrete subgroups would be adequate for quantum simulations.

This paper is organized as follows. In Sec. II, we present the group-theoretic details of $\Sigma(36 \times 3)$ and the digitization scheme. A summary of the qudit gates used is found in Sec. III. Sec. IV briefly reviews the necessary primitive gates for gauge theories, and then explicit circuits for $\Sigma(72 \times 3)$ are derived in the following sections: the inversion gate in Sec. V, the multiplication gate in Sec. VI, the trace gate in Sec. VII, and the Fourier transform gate in Sec. VIII. Using these gates, we discuss the resource costs for simulating pure gauge $SU(3)$ in $3+1d$ in Sec. IX. We conclude and discuss future work in Sec. X.

II. GROUP PROPERTIES

In this section, we overview the properties of $\Sigma(72 \times 3)$. This discussion includes the generating representation

TABLE II. Character table of $\Sigma(72 \times 3)$ with $\omega = e^{2\pi i/3}$ adapted from [107].

Size	1	1	1	24	9	9	9	18	18	18	18	18	18	18	18
Ord	1	3	3	3	2	6	6	4	12	12	4	12	12	12	12
$\mathbf{1}^{(0)}$	1	1	1	1	1	1	1	1	1	1	1	1	1	1	1
$\mathbf{1}^{(1)}$	1	1	1	1	1	1	1	-1	-1	-1	1	1	1	-1	-1
$\mathbf{1}^{(2)}$	1	1	1	1	1	1	1	1	1	1	-1	-1	-1	-1	-1
$\mathbf{1}^{(3)}$	1	1	1	1	1	1	1	-1	-1	-1	-1	-1	-1	1	1
$\mathbf{2}$	2	2	2	2	-2	-2	-2	0	0	0	0	0	0	0	0
$\mathbf{3}^{(0)}$	3	3ω	$3\omega^2$	0	-1	$-\omega$	$-\omega^2$	1	ω	ω^2	1	ω	ω^2	ω	ω^2
$\mathbf{3}^{(1)}$	3	3ω	$3\omega^2$	0	-1	$-\omega$	$-\omega^2$	-1	$-\omega$	$-\omega^2$	1	ω	ω^2	$-\omega$	$-\omega^2$
$\mathbf{3}^{(2)}$	3	3ω	$3\omega^2$	0	-1	$-\omega$	$-\omega^2$	1	ω	ω^2	-1	$-\omega$	$-\omega^2$	$-\omega$	$-\omega^2$
$\mathbf{3}^{(3)}$	3	3ω	$3\omega^2$	0	-1	$-\omega$	$-\omega^2$	-1	$-\omega$	$-\omega^2$	-1	$-\omega$	$-\omega^2$	ω	ω^2
$\mathbf{3}^{(0)*}$	3	$3\omega^2$	3ω	0	-1	$-\omega^2$	$-\omega$	1	ω^2	ω	1	ω^2	ω	ω^2	ω
$\mathbf{3}^{(1)*}$	3	$3\omega^2$	3ω	0	-1	$-\omega^2$	$-\omega$	-1	$-\omega^2$	$-\omega$	1	ω^2	ω	$-\omega^2$	$-\omega$
$\mathbf{3}^{(2)*}$	3	$3\omega^2$	3ω	0	-1	$-\omega^2$	$-\omega$	1	ω^2	ω	-1	$-\omega^2$	$-\omega$	$-\omega^2$	$-\omega$
$\mathbf{3}^{(3)*}$	3	$3\omega^2$	3ω	0	-1	$-\omega^2$	$-\omega$	-1	$-\omega^2$	$-\omega$	-1	$-\omega^2$	$-\omega$	ω^2	ω
$\mathbf{6}$	6	6ω	$6\omega^2$	0	2	2ω	$2\omega^2$	0	0	0	0	0	0	0	0
$\mathbf{6}^*$	6	$6\omega^2$	6ω	0	2	$2\omega^2$	2ω	0	0	0	0	0	0	0	0
$\mathbf{8}$	8	8	8	-1	0	0	0	0	0	0	0	0	0	0	0

used, the irreducible representations, and how the digitization is mapped onto qubit-based platforms. The group has the following generators:

$$\begin{aligned}
 C &= \begin{pmatrix} 1 & 0 & 0 \\ 0 & \omega & 0 \\ 0 & 0 & \omega^2 \end{pmatrix}; & V &= \frac{1}{\sqrt{3}i} \begin{pmatrix} 1 & 1 & 1 \\ 1 & \omega & \omega^2 \\ 1 & \omega^2 & \omega \end{pmatrix} \\
 E &= \begin{pmatrix} 0 & 1 & 0 \\ 0 & 0 & 1 \\ 1 & 0 & 0 \end{pmatrix}; & X &= \frac{1}{\sqrt{3}i} \begin{pmatrix} 1 & 1 & \omega^2 \\ 1 & \omega & \omega \\ \omega & 1 & \omega \end{pmatrix} \quad (1)
 \end{aligned}$$

with $\omega = e^{2\pi i/3}$. These matrices are in the faithful $SU(3)$ representations of $\Sigma(72 \times 3)$ and have the properties

$$\begin{aligned}
 XC &= C^2EX, & XE &= \omega^2CEX \\
 XV &= \omega^2EV^3X & C^3 &= E^3 = V^4 = X^4 = \mathbb{1}. \quad (2)
 \end{aligned}$$

With these, any element g of $\Sigma(72 \times 3)$ can be written as

$$g = \omega^p C^q E^r V^{2s+t} X^u, \quad (3)$$

where $0 \leq p, q, r \leq 2$ and $0 \leq s, t, u \leq 1$. For hybrid qudit platforms, the natural encoding to minimize errors would be three qutrits and three qubits [108]. For qubit platforms, we expand each of p, q, r, y into two binary variables. Thus, Eq. (3) becomes

$$g = \omega^{p_1+2p_2} C^{q_1+2q_2} E^{r_1+2r_2} V^{2s+t} X^u,$$

where each variable is binary. It is necessary to restrict the variables due to excess of qubit states: $\lambda_1 + \lambda_2 \leq 1$ for $\lambda = p, q, r$. Thus, a $\Sigma(72 \times 3)$ -register requires 9 qubits and

is given by the binary encoding in the $|utsr_1r_0q_1q_0p_1p_0\rangle$. We use $|N\rangle$ to denote this encoding where N is the integer representation of the binary string. For example,

$$\frac{i}{\sqrt{3}} \begin{pmatrix} \omega^2 & \omega & \omega \\ 1 & \omega & 1 \\ 1 & 1 & \omega \end{pmatrix} = \omega^{1+2 \times 0} C^{0+2 \times 1} E^{1+2 \times 0} V^{2 \times 0+1} X^1 \\ \rightarrow |110011001\rangle = |409\rangle \quad (4)$$

The group $\Sigma(72 \times 3)$ has 16 irreducible representations (irreps): $\mathbf{1}^{(a)}$, $\mathbf{2}$, $\mathbf{3}^{(a)}$, $\mathbf{3}^{(a)*}$, $\mathbf{6}$, $\mathbf{6}^*$, and $\mathbf{8}$ where $0 \leq a \leq 3$. The bold faced numbers indicate the dimension and the superscripts differentiate the various irreps in a given dimension. Using character table (Tab. II) and Eq. (2) one can identify a presentation denoted $\rho_i(g)$ for each irrep i . These are for the 1d irreps:

$$\begin{aligned} \rho_{\mathbf{1}^{(0)}}(g) &= 1; & \rho_{\mathbf{1}^{(1)}}(g) &= (-1)^t; \\ \rho_{\mathbf{1}^{(2)}}(g) &= (-1)^u; & \rho_{\mathbf{1}^{(3)}}(g) &= (-1)^{t+u}; \end{aligned} \quad (5)$$

the 2d irrep:

$$\rho_{\mathbf{2}}(g) = \begin{pmatrix} 0 & -i \\ -i & 0 \end{pmatrix}^{2s+t} \begin{pmatrix} 0 & 1 \\ -1 & 0 \end{pmatrix}^u \quad (6)$$

Using ω , C , E , V , and X from Eq. (1), the 3d irreps are

$$\begin{aligned} \rho_{\mathbf{3}^{(0)}}(g) &= \omega^p C^q E^r V^{2s+t} X^u \\ \rho_{\mathbf{3}^{(1)}}(g) &= \omega^p C^q E^r (-V)^{2s+t} X^u \\ \rho_{\mathbf{3}^{(2)}}(g) &= \omega^p C^q E^r V^{2s+t} (-X)^u \\ \rho_{\mathbf{3}^{(3)}}(g) &= \omega^p C^q E^r (-V)^{2s+t} (-X)^u. \end{aligned} \quad (7)$$

The 3d conjugate representations correspond to $V, X \rightarrow \bar{V}, \bar{X}$. The 6d irreducible representation is:

$$\begin{aligned} \rho_{\mathbf{6}}(\omega) &= e^{2\pi i/3}; \\ \rho_{\mathbf{6}}(C) &= \rho_{\mathbf{3}^{(0)}}(C) \oplus (\omega^2 \rho_{\mathbf{3}^{(0)}}(C^2)); \\ \rho_{\mathbf{6}}(E) &= \rho_{\mathbf{3}^{(0)}}(E) \oplus \rho_{\mathbf{3}^{(0)}}(E^2); \end{aligned}$$

$$\rho_{\mathbf{6}}(V) = -\frac{1}{3} \begin{pmatrix} 1 & 1 & 1 & \sqrt{2} & \sqrt{2} & \sqrt{2} \\ 1 & \omega^2 & \omega & \sqrt{2}\omega & \sqrt{2}\omega^2 & \sqrt{2} \\ 1 & \omega & \omega^2 & \sqrt{2}\omega^2 & \sqrt{2}\omega & \sqrt{2} \\ \sqrt{2} & \sqrt{2}\omega & \sqrt{2}\omega^2 & \omega+1 & \omega^2+1 & -1 \\ \sqrt{2} & \sqrt{2}\omega^2 & \sqrt{2}\omega & \omega^2+1 & \omega+1 & -1 \\ \sqrt{2} & \sqrt{2} & \sqrt{2} & -1 & -1 & -1 \end{pmatrix};$$

$$\rho_{\mathbf{6}}(X) = -\frac{1}{3} \begin{pmatrix} 1 & 1 & \omega & \sqrt{2} & \sqrt{2}\omega^2 & \sqrt{2}\omega^2 \\ 1 & \omega^2 & \omega^2 & \sqrt{2}\omega & \sqrt{2}\omega & \sqrt{2}\omega^2 \\ \omega^2 & 1 & \omega^2 & \sqrt{2}\omega & \sqrt{2}\omega^2 & \sqrt{2}\omega \\ \sqrt{2} & \sqrt{2}\omega & \sqrt{2} & \omega+1 & -1 & -\omega^2 \\ \sqrt{2}\omega & \sqrt{2} & \sqrt{2} & \omega+1 & \omega+1 & -1 \\ \sqrt{2}\omega & \sqrt{2}\omega & \sqrt{2}\omega^2 & -\omega & -1 & -1 \end{pmatrix};$$

for its conjugate $\rho_{\mathbf{6}^*}(g) = (\rho_{\mathbf{6}}(g))^*$. The 8d irrep is

$$\rho_{\mathbf{8}}(\omega)=1; \quad \rho_{\mathbf{8}}(C) = \begin{pmatrix} -\frac{1}{2} & -\frac{\sqrt{3}}{2} & 0 \\ \frac{\sqrt{3}}{2} & -\frac{1}{2} & 0 \\ 0 & 0 & 1 \end{pmatrix} \oplus \begin{pmatrix} -\frac{1}{2} & \frac{\sqrt{3}}{2} \\ -\frac{\sqrt{3}}{2} & -\frac{1}{2} \end{pmatrix} \oplus \begin{pmatrix} -\frac{1}{2} & -\frac{\sqrt{3}}{2} & 0 \\ \frac{\sqrt{3}}{2} & -\frac{1}{2} & 0 \\ 0 & 0 & 1 \end{pmatrix}; \quad \rho_{\mathbf{8}}(E) = \begin{pmatrix} 0 & 0 & 0 & 0 & 1 & 0 & 0 & 0 \\ 0 & 0 & 0 & 0 & 0 & 1 & 0 & 0 \\ 0 & 0 & -\frac{1}{2} & 0 & 0 & 0 & \frac{\sqrt{3}}{2} & 0 \\ 0 & 0 & 0 & 0 & 0 & 0 & 1 & 0 \\ 1 & 0 & 0 & 0 & 0 & 0 & 0 & 0 \\ 0 & -1 & 0 & 0 & 0 & 0 & 0 & 0 \\ 0 & 0 & 0 & 1 & 0 & 0 & 0 & 0 \\ 0 & 0 & -\frac{\sqrt{3}}{2} & 0 & 0 & 0 & -\frac{1}{2} & 0 \end{pmatrix};$$

$$\rho_{\mathbf{8}}(V) = \begin{pmatrix} \frac{1}{6} & -\frac{1}{2\sqrt{3}} & \frac{1}{2} & \frac{1}{6} & \frac{1}{2\sqrt{3}} & -\frac{1}{3} & \frac{1}{\sqrt{3}} & \frac{1}{2\sqrt{3}} \\ \frac{1}{2\sqrt{3}} & -\frac{1}{2} & -\frac{1}{2\sqrt{3}} & -\frac{1}{2\sqrt{3}} & -\frac{1}{2} & 0 & 0 & \frac{1}{2} \\ \frac{1}{2} & \frac{1}{2\sqrt{3}} & 0 & \frac{1}{2} & -\frac{1}{2\sqrt{3}} & \frac{1}{2} & \frac{1}{2\sqrt{3}} & 0 \\ \frac{1}{6} & \frac{1}{2\sqrt{3}} & \frac{1}{2} & \frac{1}{6} & -\frac{1}{2\sqrt{3}} & -\frac{1}{3} & -\frac{1}{\sqrt{3}} & \frac{1}{2\sqrt{3}} \\ -\frac{1}{2\sqrt{3}} & -\frac{1}{2} & \frac{1}{2\sqrt{3}} & \frac{1}{2\sqrt{3}} & -\frac{1}{2} & 0 & 0 & -\frac{1}{2} \\ -\frac{1}{3} & 0 & \frac{1}{2} & -\frac{1}{3} & 0 & \frac{2}{3} & 0 & \frac{1}{2\sqrt{3}} \\ -\frac{1}{\sqrt{3}} & 0 & -\frac{1}{2\sqrt{3}} & \frac{1}{\sqrt{3}} & 0 & 0 & 0 & \frac{1}{2} \\ \frac{1}{2\sqrt{3}} & -\frac{1}{2} & 0 & \frac{1}{2\sqrt{3}} & \frac{1}{2} & \frac{1}{2\sqrt{3}} & -\frac{1}{2} & 0 \end{pmatrix}; \quad \rho_{\mathbf{8}}(X) = \begin{pmatrix} \frac{1}{6} & -\frac{1}{2\sqrt{3}} & \frac{1}{2} & -\frac{1}{3} & 0 & -\frac{1}{3} & -\frac{1}{\sqrt{3}} & \frac{1}{2\sqrt{3}} \\ \frac{1}{2\sqrt{3}} & -\frac{1}{2} & -\frac{1}{2\sqrt{3}} & \frac{1}{\sqrt{3}} & 0 & 0 & 0 & \frac{1}{2} \\ \frac{1}{2} & \frac{1}{2\sqrt{3}} & 0 & 0 & \frac{1}{\sqrt{3}} & -\frac{1}{2} & \frac{1}{2\sqrt{3}} & 0 \\ \frac{1}{6} & \frac{1}{2\sqrt{3}} & -\frac{1}{2} & -\frac{1}{3} & -\frac{1}{\sqrt{3}} & -\frac{1}{3} & 0 & \frac{1}{2\sqrt{3}} \\ \frac{1}{2\sqrt{3}} & \frac{1}{2} & \frac{1}{2\sqrt{3}} & 0 & 0 & \frac{1}{\sqrt{3}} & 0 & \frac{1}{2} \\ \frac{2}{3} & 0 & 0 & \frac{1}{6} & -\frac{1}{2\sqrt{3}} & \frac{1}{6} & -\frac{1}{2\sqrt{3}} & -\frac{1}{\sqrt{3}} \\ 0 & 0 & \frac{1}{\sqrt{3}} & \frac{1}{2\sqrt{3}} & -\frac{1}{2} & -\frac{1}{2\sqrt{3}} & \frac{1}{2} & 0 \\ \frac{1}{2\sqrt{3}} & -\frac{1}{2} & 0 & -\frac{1}{\sqrt{3}} & 0 & \frac{1}{2\sqrt{3}} & \frac{1}{2} & 0 \end{pmatrix}.$$

$\mathbf{1}^{(a)}$ and $\mathbf{2}$ are connected with the finite subgroup \mathbb{Q}_8 of $SU(2)$. Further, the various 3d irreps are connected to the \mathbb{Q}_8 structure. $\mathbf{6}$ mixes a subset of the $\Sigma(36 \times 3)$ 3d irreps while $\mathbf{8}$ mixes the two 4d irreps of $\Sigma(36 \times 3)$ [91].

III. QUBIT & QUTRIT GATES

The implementation of our group primitive gates requires defining a set of quantum gate operations. We choose a universal set which includes some redundancy in order to compactly represent our circuits. We use the Pauli gates ($p = X, Y, Z$) and their arbitrary rotations generalizations $R_p(\theta) = e^{ip\theta/2}$. How these are decomposed in terms of the $T = \text{diag}(1, e^{i\pi/4})$ gate becomes relevant to fault-tolerant resource estimations. We further use a few two-qubit gates. The SWAP gate exchanges the state of two qubits, while the CNOT gate is defined by

$$\text{CNOT} |a\rangle \otimes |b\rangle = |a\rangle \otimes |b \oplus a\rangle,$$

where \oplus indicates addition modulo 2. We further use the multi-controlled gates such as the C^n NOT and CSWAP (Fredkin) gate. The effect of C^2 NOT (Toffoli) on a quantum state is

$$C^2\text{NOT} |a\rangle \otimes |b\rangle \otimes |c\rangle = |a\rangle \otimes |b\rangle \otimes |c \oplus ab\rangle.$$

The CSWAP gate exchanges two qubits based on the control, and written in terms of modular arithmetic is

$$\begin{aligned} \text{CSWAP} |a\rangle \otimes |b\rangle \otimes |c\rangle &= |a\rangle \otimes |b(1 \oplus a) \oplus ac\rangle \\ &\otimes |c(1 \oplus a) \oplus ab\rangle. \end{aligned}$$

Since several of the generators have order 3, it is useful to consider hybrid encodings with qutrits as an intermediate step. As such, we use a number of qutrit gates in this paper. The single-qudit rotations are denoted by $R_\alpha^{(i,j)}(\theta)$, where $\alpha = \{X, Y, Z\}$ and indicate a Pauli rotation between levels i and j . Further, we use the two-qudit entangling gate,

$$C_a^i X_b^{(j,k)}, \quad (8)$$

which corresponds to the CNOT operation controlled on state i of qutrit a , and targets qutrit b with an X operation between the levels j and k . Another important qudit gate, χ represents the increment gate, which takes

$$\chi |a\rangle = |a \oplus_d 1\rangle \quad (9)$$

where d indicates the dimension of the qudit as well as the modulus of the addition. In this work, we only consider the qutrit χ :

$$\chi = \begin{pmatrix} 0 & 0 & 1 \\ 1 & 0 & 0 \\ 0 & 1 & 0 \end{pmatrix} \quad (10)$$

which can be decomposed into two-qubit registers as

$$\chi |a\rangle |b\rangle = (C_b X_a)(C_a X_b)(X \otimes \mathbf{1}) |a\rangle |b\rangle \quad (11)$$

We also for conciseness consider the CSUM gate:

$$\text{CSUM}_{a,b} |i\rangle_a |j\rangle_b = |i\rangle_a |i \oplus_3 j\rangle_b. \quad (12)$$

with a control qudit a and target qutrit b and can be constructed from $C_a^i X_b^{(j,k)}$ by [109]:

$$\text{CSUM}_{a,b} = (C_a^1 X_b^{(0,1)} C_a^1 X_b^{(1,2)})(C_a^2 X_b^{(1,2)} C_a^2 X_b^{(0,1)}). \quad (13)$$

Further generalizations used are the multi-controlled versions of these gates e.g. $C_a^i C_b^j X_c^{(k,l)}$ and

$$\text{CCSUM}_{a,b,c} |i\rangle_a |j\rangle_b |k\rangle_c = |i\rangle_a |j\rangle_b |k \oplus_3 ij\rangle_c. \quad (14)$$

With these, there are several decompositions from qutrit-qubits operators to pure qubit ones summarize in App. A. Specifically, the number of control qutrits can be reduced with the Toffoli staircase decomposition [110–112].

IV. OVERVIEW OF PRIMITIVE GATES

In Ref. [97], the Hamiltonian simulations of lattice gauge theories can be constructed from a set of group-theoretic primitive gates. This reduces the problem of simulation to constructing these primitive gates and estimating their cost. One choice of primitive gates is: inversion (\mathfrak{U}_{-1}), multiplication (\mathfrak{U}_\times), trace (\mathfrak{U}_{Tr}), Fourier transformation (\mathfrak{U}_F), Fourier phase ($\mathfrak{U}_\phi(\theta)$), and gauge-matter interaction ($\mathfrak{U}_{gm}(\theta)$). In this work we will consider all but the gauge-matter interaction, which we leave for future work.

\mathfrak{U}_{-1} and \mathfrak{U}_\times permute group element basis states by

$$\mathfrak{U}_{-1} |g\rangle = |g^{-1}\rangle \quad (15)$$

and

$$\mathfrak{U}_\times |g\rangle \otimes |h\rangle = |g\rangle |gh\rangle. \quad (16)$$

This left multiplication is sufficient however an explicit right multiplication gate can further reduce costs [90].

Hamiltonian simulations of lattice gauge theories also require applying phases proportional to the real part of traces:

$$\mathfrak{U}_{\text{Tr}}(\theta) |g\rangle = e^{i\theta \text{Re}(\text{Tr}(g))}. \quad (17)$$

The final two gates of this set are \mathfrak{U}_F and $\mathfrak{U}_\phi(\theta)$. For a finite group G , the *discrete Fourier transform* (DFT) can be defined as \hat{f} , of a function f over a finite G is

$$\hat{f}(\rho) = \sum_{g \in G} \sqrt{\frac{d_\rho}{|G|}} f(g) \rho(g), \quad (18)$$

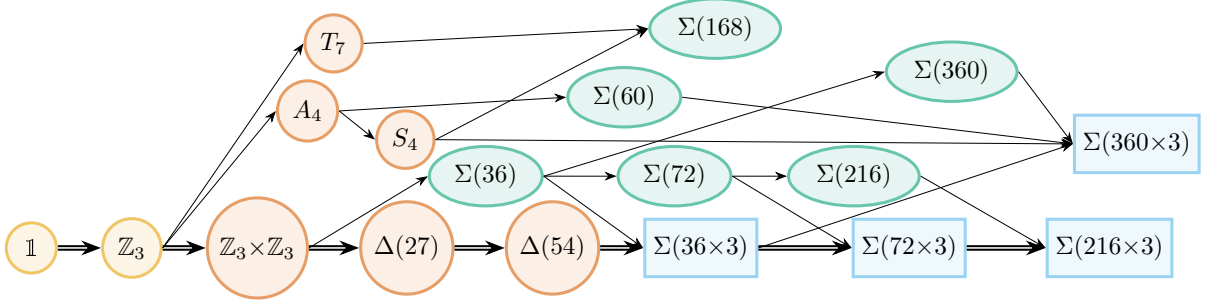


FIG. 2. Lattice of subgroups of $SU(3)$. Each path represents a possible decomposition of \mathfrak{U}_{FFT}^G . The double-line path indicates the one explored in this work.

where $|G|$ is the size of the group, d_ρ is the dimensionality of the irrep ρ . With the dual \hat{G} is the set of irreps of G , \mathfrak{U}_F acts on a single G -register with some amplitudes $f(g)$ to rotate it into the irrep basis:

$$\mathfrak{U}_{FT} \sum_{g \in G} f(g) |g\rangle = \sum_{\rho \in \hat{G}} \hat{f}(\rho)_{ij} |\rho, i, j\rangle. \quad (19)$$

Naively constructing the DFT requires $O(|G|)$ gates. Instead we construct a fast Fourier transform (FFT), reducing the complexity to $O(|G| \log(G))$. Such quantum FFTs \mathfrak{U}_{FFT}^G have been constructed for a number of finite groups [113–119]. The procedure for deriving \mathfrak{U}_{FFT}^G involves extending Fourier transforms along a series of nested subgroups [116, 118, 120]. There are numerous paths that can be taken, given by the lattice of subgroups (See Fig 2).

Depending on the specifics of the discrete group, different constructions are possible, but here we follow Püschel et al.’s method [118]. The algorithm works by appending a list of elements, denoted a *right transversal*, to an existing group whose Fourier transform is known, e.g. \mathbb{Z}_3 , and then using the effects of the right transversal to extend the irreps of the subgroup to those of a parent group, e.g. $\mathbb{Z}_3 \times \mathbb{Z}_3$ or A_4 .

To do this, one decomposes \mathfrak{U}_{FFT}^G into six subroutines at each recursive step. They are: \mathfrak{U}_{FFT}^H of a subgroup $H \in G$, two irrep permutations (P and C), a twiddle matrix (\mathfrak{D}), a cyclic FFT over the transversal (DFT), and a phase-kickback operation (Φ^H).

When performing \mathfrak{U}_{FFT}^H , the irrep basis is often not aligned with that of G , thus one uses P and C to permute the subgroup irreps. P permutes the irreps such that they are easily identifiable. Then C permutes irreps which are not invariant under conjugation by the transversal, i.e. $\rho^\alpha(tgt^{-1}) \neq \rho^\alpha$. This reduces the cost and complexity for the later phase-kickback operation, Φ .

The twiddle operation, T is controlled by a transversal register and performs two functions. It either mixes conjugate irreps to make a larger dimensional irrep or transforms an existing irrep into the desired representation. This is followed by DFT on the transversal register which mixes the irreps and ensures that the transversal

component is moved to the irrep basis. The final step involves a phase kickback that applies certain phases to irreps to preclude isomorphism from existing. The structure for a quantum Fourier transform is shown in Fig. 3.

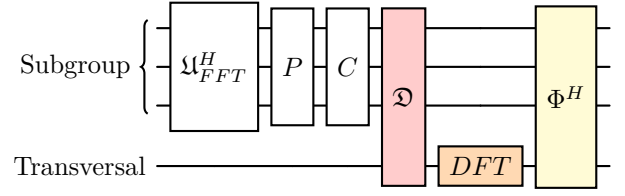


FIG. 3. Schematic of the \mathfrak{U}_{FFT}^G provided in Ref. [118].

The final primitive, $\mathfrak{U}_\phi(\theta)$ corresponds to a diagonal phasing operation on the various qubits corresponding to the eigenvalues of the various irreps of the kinetic term of the Hamiltonian.

V. INVERSION GATES

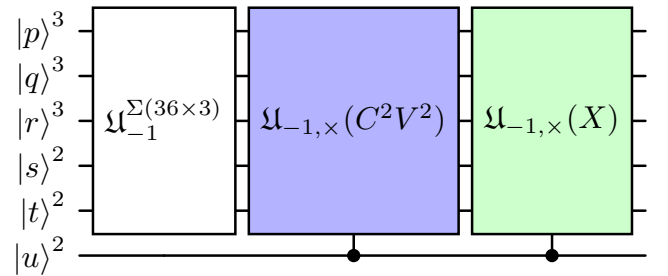


FIG. 4. Diagrammatic formulation of $\mathfrak{U}_{-1}^{\Sigma(72 \times 3)}$ with $\mathfrak{U}_{-1}^{\Sigma(36 \times 3)}$ from [103] and the remaining gates defined in Fig. 5 and 6.

The inversion operations $\mathfrak{U}_{-1}^{\Sigma(72 \times 3)}$ can be written in a structured recursive way as shown in Fig. 4 which relies on the inversion gate of $\Sigma(36 \times 3)$. To derive this, first one establishes the inversion relation rules for the bit-strings $pqrstu$. This starts by identifying what happens to the

group element $g \in \Sigma(72 \times 3)$ in Eq. (3) under inversion:

$$\begin{aligned} g^{-1} &= X^{-u} V^{2(s+t)+t} E^{2r} C^{2q} \omega^{2p} \\ &= X^u C^{2u} V^{2u} (\omega^{p'} C^{q'} E^{r'} V^{2s'+t'}) \end{aligned} \quad (20)$$

where p' , q' , r' , s' , and t' are after application of $\mathfrak{U}_{-1}^{\Sigma(36 \times 3)}$ found in [103]. The next step, which we will implement as the gate $\mathfrak{U}_{\times}(C^2V^2)$, involves propagating the $C^{2u}V^{2u}$ through the remainder of the expression to get:

$$g^{-1} = X^u \omega^{p''} C^{q''} E^{r''} V^{2s''+t''} \quad (21)$$

where since ω commutes and V^{2u} is squared $p'' = p'$ and $t'' = t'$ are unaffected leaving:

$$\begin{aligned} q'' &= q'(1-u) + 2u(q'+1) \\ r'' &= r'(1-u) + 2ur' \\ s'' &= (s'+u) \end{aligned} \quad (22)$$

To proceed further, one pushes the X^u through the remaining elements. The associated gate we call $\mathfrak{U}_{\times}(X)$ and has three steps. Propagating X^u first through the $C^{q''}E^{r''}$ terms yields $g^{-1} = \omega^{p'''} C^{q'''} E^{r'''} X^u V^{2s''' + t'''}$ with

$$\begin{aligned} p''' &= p'' + u(2\delta_{q',2} + 2\delta_{r,1} + 2\delta_{r',2} + q'r') \\ q''' &= q''(1-u) + (2q'' + r'')u \\ r''' &= r'' + q''u \end{aligned} \quad (23)$$

with $s''' = s''$, $t''' = t''$ unchanged. Going through V^{2s} gives $g^{-1} = \omega^{\tilde{p}} C^{\tilde{q}} E^{\tilde{r}} V^{2\tilde{s} + \tilde{t}} X^u V^{\tilde{t}}$

$$\begin{aligned} \tilde{p} &= p''' + 2us''' + us'''r''' \\ \tilde{q} &= q''' + s'''u \\ \tilde{r} &= r''' + s'''u \\ \tilde{s} &= s''' \end{aligned} \quad (24)$$

while leaving $\tilde{t} = t'''$ untouched. The final push through $V^{\tilde{t}}$ give $g^{-1} = \omega^{\bar{p}} C^{\bar{q}} E^{\bar{r}} V^{2\bar{s} + \bar{t}} X^{\bar{u}}$ which interestingly changed neither $\bar{t} = \tilde{t}$ nor $\bar{u} = u$ but instead:

$$\begin{aligned} \bar{p} &= \tilde{p} + 2u\tilde{t} \\ \bar{q} &= \tilde{q} \\ \bar{r} &= \tilde{r} + u\tilde{t}(1-\tilde{s}) + 2u\tilde{t}\tilde{s} \\ \bar{s} &= \tilde{s} + u\tilde{t} \end{aligned} \quad (25)$$

The explicit circuit which performs $\mathfrak{U}_{\times}(C^2V^2)$ and $\mathfrak{U}_{\times}(X)$ are provided in Fig. 5. One can convert this qutrit-qubit into the purely qubit gate shown in Fig. 6 using the methods of Appendix A.

VI. MULTIPLICATION GATES

The group multiplication gate uses a similar recursive decomposition to \mathfrak{U}_{-1} by breaking it into two gates:

$$\mathfrak{U}_{\times}^{\Sigma(72 \times 3)} = \mathfrak{U}_{\times}^{\Sigma(36 \times 3)} \mathfrak{U}_{\times, X}. \quad (26)$$

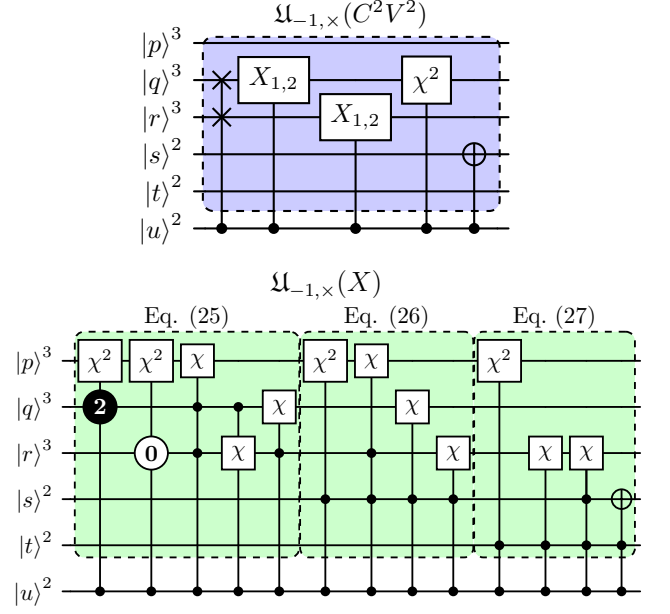


FIG. 5. Decomposition for (top) $\mathfrak{U}_{-1, \times}(C^2V^2)$ and (bottom) $\mathfrak{U}_{-1, \times}(X)$ (right) into qubit-qutrit gates which appear in the circuit decomposition of Fig. 4.

The circuit for $\mathfrak{U}_{\times}^{\Sigma(36 \times 3)}$ is found in [103]. The additional $\mathfrak{U}_{\times, X}$ are modifications gates which appear earlier in the inversion procedure. To start, given group elements

$$\begin{aligned} g &= \omega^{p_g} C^{q_g} E^{r_g} V^{2s_g + t_g} X^{u_g} \\ h &= \omega^{p_h} C^{q_h} E^{r_h} V^{2s_h + t_h} X^{u_h} \end{aligned}$$

the product of the two elements can be written as

$$hg = \omega^{\bar{p}} C^{\bar{q}} E^{\bar{r}} V^{2\bar{s} + \bar{t}} X^{\bar{u}} \quad (27)$$

where we need to determine the exponents. The first step propagates $X^{u'}$ yielding the same $\mathfrak{U}_{-1, \times}(X)$ except controlled on $|u_h\rangle$. For the case of $u_g = 2$, the application of $\mathfrak{U}_{-1, \times}(X)$ alone is insufficient in the case where $u_h = u'_g = 1$, as it produces an additional C^2V^2 :

$$hg = \omega^{p'_g} C^{q'_g} E^{r'_g} V^{2s'_g + t'_g} C^{2u_h u_g} V^{2u_h u_g} X^{u_g \oplus u_h} \quad (28)$$

which must then be propagated into place, giving

$$\begin{aligned} p''_g &= p'_g \oplus_3 r'_g u_g u_h (1 - t'_g) (s'_g \oplus_3 2(1 - s'_g)) \\ q''_g &= q'_g \oplus_3 u_g u_h (1 - t'_g) (s'_g \oplus_3 2(1 - s'_g)) \\ r''_g &= r'_g \oplus_3 u_g u_h t'_g (2(1 - s'_g) \oplus_3 s'_g) \\ s''_g &= s'_g \oplus_2 s u_g u_h \\ t''_g &= t'_g \\ u''_g &= u_g \oplus_2 s u_h \end{aligned} \quad (29)$$

After this, the remaining operations are equivalent to $\mathfrak{U}_{\times}^{\Sigma(36 \times 3)}$ which can be performed following [103]. The qutrit-qubit circuit is shown in Fig. 7, while the qubit circuit is provided in Fig. 8.

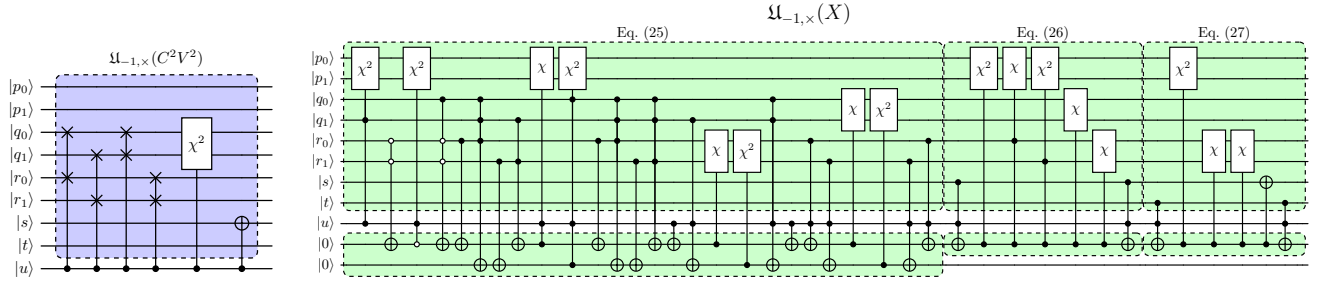


FIG. 6. Decomposition of the intermediate controlled inversion gates (left) $\mathfrak{U}_{-1,\times}(C^2V^2)$ and (right) $\mathfrak{U}_{-1,\times}(X)$. The control is explicitly on the $|u\rangle$ state and the target qubits are ancilla registers and the $\Sigma(36 \times 3)$ subgroup.

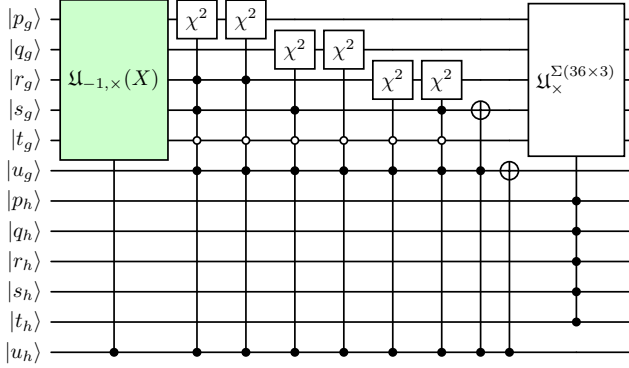


FIG. 7. Qutrit-Qubit decomposition of $\mathfrak{U}_x^{\Sigma(72 \times 3)}$. $\mathfrak{U}_{-1,\times}(X)$ is shown in Fig. 4 except the control is $|u_h\rangle$ instead of $|u_g\rangle$ while $\mathfrak{U}_x^{\Sigma(36 \times 3)}$ is provided in Ref. [103].

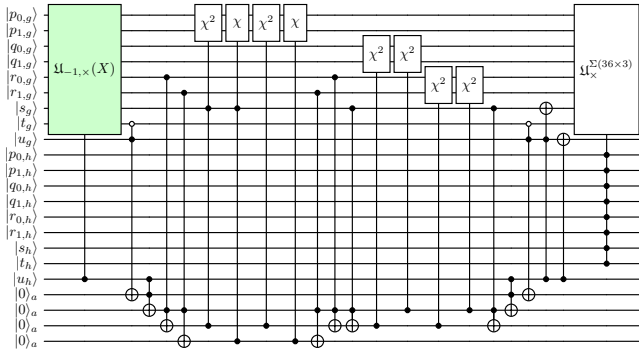


FIG. 8. Qubit decomposition of $\mathfrak{U}_x^{\Sigma(72 \times 3)}$. $\mathfrak{U}_{-1,\times}(X)$ is shown in Fig. 6 except the control is $|u_h\rangle$ instead of $|u_g\rangle$.

VII. TRACE GATES

The trace gate \mathfrak{U}_{Tr} for a discrete group can be decomposed into two components: $\mathfrak{U}_{\text{squish}}^G$ and $\mathfrak{U}_{\text{Tr}}^G(\phi)$. The circuits $\mathfrak{U}_{\text{squish}}^G$ and its conjugate compute and uncompute the associated trace class for g onto an ancilla register. With this identification, $\mathfrak{U}_{\text{Tr}}^G$ implements a small Hamiltonian on the ancilla register to get the correct phase rotation. A schematic for \mathfrak{U}_{Tr} is provided in Fig. 9.

To construct \mathfrak{U}_{Tr} , we need to construct a map from

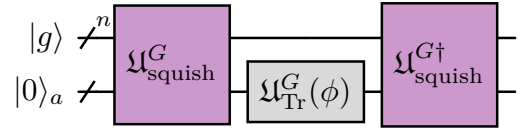


FIG. 9. Schematic of \mathfrak{U}_{Tr} for an arbitrary group G . The $\mathfrak{U}_{\text{squish}}^G$ maps the group elements to the real values of the trace classes and the gate $\mathfrak{U}_{\text{Tr}}^G(\phi)$ phases the group elements depending on their real values of the fiducial trace.

g to their respective trace classes found in Tab. II. For $\Sigma(72 \times 3)$, the real portion of the trace for the classes are identical to those of $\Sigma(36 \times 3)$: $\{3, -\frac{3}{2}, 0, \pm 1, \pm \frac{1}{2}\}$ and how each trace is mapped into the ancilla is in Tab. III.

TABLE III. Map for the group elements to ancilla register for $\Sigma(72 \times 3)$. This mapping is the same as that for $\Sigma(36 \times 3)$.

$\text{Re}(\text{Tr}(g))$	3	$-\frac{3}{2}$	-1	$-\frac{1}{2}$	0	1	$\frac{1}{2}$
v_0	0	1	0	1	0	1	0
v_1	0	0	1	1	0	0	1
v_2	0	0	0	0	1	1	1

Using Tab. III, the $\mathfrak{U}_{\text{Tr}}^{\Sigma(72 \times 3)}(\phi)$ is shown in Fig. 10 and is same as the one for $\Sigma(36 \times 3)$ from [103].

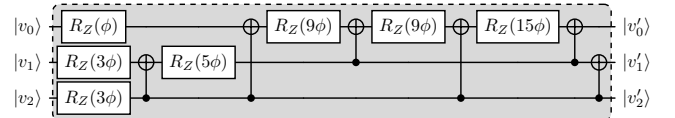


FIG. 10. Implementation of $\mathfrak{U}_{\text{Tr}}^{\Sigma(72 \times 3)}(\phi)$.

The difference with $\Sigma(72 \times 3)$ is that there are additional conjugacy classes that need to be mapped to

$|v_2v_1v_0\rangle$. The extra conjugacy classes we need are:

$$\begin{aligned}
C_X &= \{X, \omega^2 V^2 X, \omega^2 E^2 V^2 X, \omega^2 C^2 E V^2 X, \omega C^2 X, \\
&\quad \omega E V^2 X, C^2 V^2 X, \omega C X, \omega^2 C V^2 X, \omega^2 C E^2 V^2 X, \\
&\quad \omega E X, \omega C E V^2 X, \omega C^2 E X, C^2 E^2 V^2 X, \\
&\quad C E^2 X, \omega^2 C^2 E^2 X, C E X, E^2 X\}, \\
C_{VX} &= \{V X, C V^3 X, \omega C E V^3 X, \omega^2 C^2 E V^3 X, \omega^2 E V X, \\
&\quad \omega^2 C^2 V X, C E^2 V^3 X, \omega C^2 E^2 V^3 X, \omega^2 C E V X, \\
&\quad \omega C E^2 V X, \omega E^2 V^3 X, \omega^2 C V X, C^2 E V X, E^2 V X, \\
&\quad \omega C^2 V^3 X, \omega V^3 X, C^2 E^2 V X, \omega^2 E V^3 X\},
\end{aligned}$$

as well as ωC_X , $\omega^2 C_X$, ωC_{VX} , and $\omega^2 C_{VX}$. We thus need to include additional maps for these classes:

$$\text{Re}(\text{Tr}(g)) \mapsto \begin{cases} -\frac{1}{2} & g \in C_{VX}, \omega C_{VX}, \omega C_X, \omega^2 C_X \\ 1 & g \in C_X, \omega^2 C_{VX} \end{cases}. \quad (30)$$

Working through the integer logic for each of the elements in Eq. (30) leads to the additional circuit structure seen in Fig. 11 for $\mathfrak{U}_{\text{squish}}^{\Sigma(72 \times 3)}$.

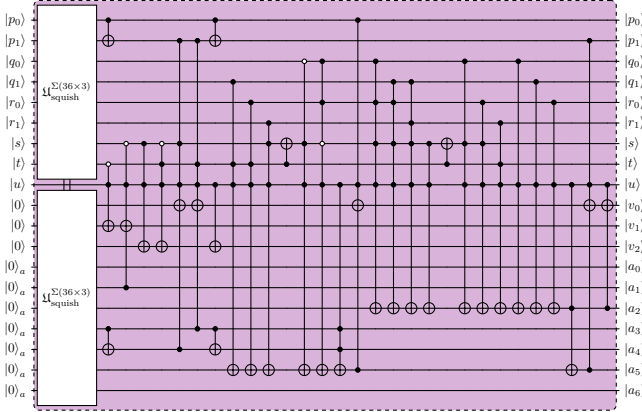


FIG. 11. Circuit for $\mathfrak{U}_{\text{squish}}^{\Sigma(72 \times 3)}$ using $\mathfrak{U}_{\text{squish}}^{\Sigma(36 \times 3)}$ from [103].

VIII. FOURIER TRANSFORMATIONS

The electric field Hamiltonian for a group G can be written

$$\begin{aligned}
\hat{H}_E &= \sum_{h \in \Gamma} \sum_{g \in G} |hg\rangle \langle g| \\
&= \sum_{\rho, m, n} f(\rho) |\rho, m, n\rangle \langle \rho, m, n|, \quad (31)
\end{aligned}$$

where $f(\rho) = |\Gamma| - \frac{1}{\dim(\rho)} \sum_{h \in \Gamma} \text{Tr}(\rho(h))$, and Γ is a subset of G subject to the constraints:

$$\begin{aligned}
\Gamma^{-1} &= \Gamma \\
g\Gamma g^{-1} &= \Gamma \quad \forall g \in G \\
1 &\notin \Gamma, \quad (32)
\end{aligned}$$

guaranteeing gauge-invariance. While the choice of Γ is not unique, the particular choice

$$\Gamma = \{g \in G \setminus \{1\} \mid \text{ReTr}(g) \text{ is maximal}\} \quad (33)$$

can be derived from the Wilson action via the transfer matrix procedure [95, 121].

Since the electric term is diagonal in the basis labeled by the irreducible representations, we will employ the Fourier transformation to move between the position basis $\{|g\rangle\}$ and the $\{|\rho, m, n\rangle\}$ basis. To this end, we will need to construct the Fourier transform quantum circuit of this group.

The construction of \mathfrak{U}_{FFT} for $\Sigma(72 \times 3)$ follows those in in [119, 122] and can be written in a block format shown in Fig. 12. The construction of a FFT relies on being able to build the twiddle matrices \mathfrak{D}_X and the phase kickback matrices $\Phi^{\Sigma(36 \times 3)}$.

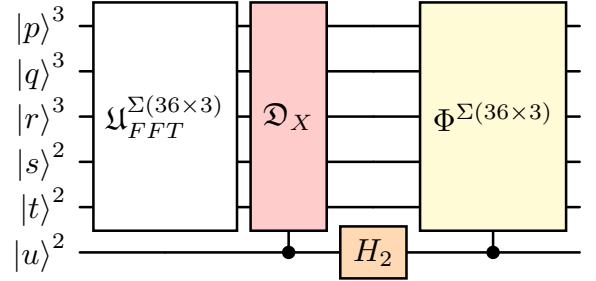


FIG. 12. Block schematic decomposition of the fast Fourier transformation for $\Sigma(72 \times 3)$.

The first step in building \mathfrak{D}_X is identifying which irreps are extendable, i.e. $\xi_{\Sigma(36 \times 3)}(X^{-1}gX) = \xi_{\Sigma(36 \times 3)}(g)$, and which ones for inner conjugates. These irreps are:

$$\xi_{1(a)}(j) = i^{a(2s+t)} \quad 0 \leq a \leq 3, \quad (34)$$

$$\xi_{3(a,b)}(j) = (-1)^{bt} \omega^{(1+b)p} C^{(1+b)q} E^r (i^a V)^{2s+t}, \quad (35)$$

where $0 \leq a \leq 3$ and $0 \leq b \leq 1$, and

$$\begin{aligned}
\xi_{4^b}(\omega) &= 1, \quad \xi_{4^b}(C) = \text{Diag}(\omega^b, \omega, \omega^{2b}, \omega^2) \\
\xi_{4^b}(E) &= \text{Diag}(\omega, \omega^{2b}, \omega^2, \omega^b) \\
\xi_{4^b}(V) &= \begin{pmatrix} 0 & 1 & 0 & 0 \\ 0 & 0 & 1 & 0 \\ 0 & 0 & 0 & 1 \\ 1 & 0 & 0 & 0 \end{pmatrix}. \quad (36)
\end{aligned}$$

We note that multiplying by X forces $s \rightarrow s + t$, meaning that the trivial irrep, $\xi_{1(0)}$, and the parity irrep $\xi_{1(2)}$ are extendable, while the other 1d irreps, $\xi_{1(1)}$ and $\xi_{1(3)}$, are a pair of inner conjugates. The 4d irreps are also a pair of inner conjugates. Similarly, the $\xi_{3(0,b)}$, $\xi_{3(2,b)}$ are extendable while, $(\xi_{3(1,b)}, \xi_{3(3,b)})$, are pairs of inner conjugates. In this way \mathfrak{D}_X induces $\mathbf{2}^{(0)}$ by mixing the irreps $\xi_{1(1)}$ and $\xi_{1(3)}$. The 3d inner conjugates further induce the $\mathbf{6}^{(0)}$ while the 4d irreps induce $\mathbf{8}$. With this, \mathfrak{D}_X is constructed following [119]. $\mathfrak{U}_{FFT}^{\Sigma(36 \times 3)}$ takes the group element basis states to the irrep basis where states are identified as follows:

$$\begin{aligned}
|0\rangle_V^2 |0\rangle_{V^2}^2 |0\rangle_E^3 |0\rangle_C^3 |0\rangle_\omega^3 &= |\xi_{1(0)}\rangle \\
|1\rangle_V^2 |0\rangle_{V^2}^2 |0\rangle_E^3 |0\rangle_C^3 |0\rangle_\omega^3 &= |\xi_{1(2)}\rangle \\
|0\rangle_V^2 |1\rangle_{V^2}^2 |0\rangle_E^3 |0\rangle_C^3 |0\rangle_\omega^3 &= |\xi_{1(1)}\rangle \\
|1\rangle_V^2 |1\rangle_{V^2}^2 |0\rangle_E^3 |0\rangle_C^3 |0\rangle_\omega^3 &= |\xi_{1(3)}\rangle \\
\{|0\rangle_V^2 |a\rangle_{V^2}^2 |b\rangle_E^3 |c\rangle_C^3 |0\rangle_\omega^3 \mid b = c \neq 0\} &= |\xi_{4(0)}\rangle \\
\{|1\rangle_V^2 |a\rangle_{V^2}^2 |b\rangle_E^3 |c\rangle_C^3 |0\rangle_\omega^3 \mid b = c \neq 0\} &= |\xi_{4(1)}\rangle \\
|0\rangle_V^2 |0\rangle_{V^2}^2 |a\rangle_E^3 |b\rangle_C^3 |1\rangle_\omega^3 &= |\xi_{3(0,0)}\rangle \\
|1\rangle_V^2 |0\rangle_{V^2}^2 |a\rangle_E^3 |b\rangle_C^3 |1\rangle_\omega^3 &= |\xi_{1(0,1)}\rangle \\
|0\rangle_V^2 |1\rangle_{V^2}^2 |a\rangle_E^3 |b\rangle_C^3 |1\rangle_\omega^3 &= |\xi_{3(2,0)}\rangle \\
|1\rangle_V^2 |1\rangle_{V^2}^2 |a\rangle_E^3 |b\rangle_C^3 |1\rangle_\omega^3 &= |\xi_{3(2,1)}\rangle \\
|0\rangle_V^2 |0\rangle_{V^2}^2 |a\rangle_E^3 |b\rangle_C^3 |2\rangle_\omega^3 &= |\xi_{3(1,0)}\rangle \\
|1\rangle_V^2 |0\rangle_{V^2}^2 |a\rangle_E^3 |b\rangle_C^3 |2\rangle_\omega^3 &= |\xi_{1(1,1)}\rangle \\
|0\rangle_V^2 |1\rangle_{V^2}^2 |a\rangle_E^3 |b\rangle_C^3 |2\rangle_\omega^3 &= |\xi_{3(3,0)}\rangle \\
|1\rangle_V^2 |1\rangle_{V^2}^2 |a\rangle_E^3 |b\rangle_C^3 |2\rangle_\omega^3 &= |\xi_{3(3,1)}\rangle.
\end{aligned} \tag{37}$$

With this identification one writes \mathfrak{D}_X :

$$\begin{aligned}
\langle 00000 | \mathfrak{D}_X | 00000 \rangle &= 1 \\
\langle 10000 | \mathfrak{D}_X | 10000 \rangle &= -1 \\
\langle t1000 | \mathfrak{D}_X | t'1000 \rangle &= \left(\rho_2(X) \right)_{t,t'} \\
\langle tsrq0 | \mathfrak{D}_X | tsr'q'0 \rangle &= \left(\rho_8(X) \right)_{3q+r-1, 3q'+r'-1} \\
q = r \neq 0; q' = r' \neq 0 \\
\langle 00rqp | \mathfrak{D}_X | 00r'q'p \rangle &= \left(\rho_{3^{(0)}}(X) \right)_{q,q'}^T; p \in \{1, 2\} \\
\langle 10rqp | \mathfrak{D}_X | 10r'q'p \rangle &= \left(\rho_{3^{(0),*}}(X) \right)_{q,q'}^T; p \in \{1, 2\} \\
\langle t10qp | \mathfrak{D}_X | t10q'p' \rangle &= \left(\rho_6(X) \right)_{3(p-1)+q, 3(p'-1)+q'} \\
p \neq 0, p' \neq 0
\end{aligned} \tag{38}$$

The quantum circuit for \mathfrak{D}_X is provided in Fig. 13 with

$$\begin{aligned}
U_{X_{8 \times 8}} &= 1 \oplus \rho_8(X) \\
U_{X_{6 \times 6}} &= \mathbb{1}_3 \oplus \rho_6(X).
\end{aligned} \tag{39}$$

$U_{X_{8 \times 8}}$ and $U_{X_{6 \times 6}}$ can be decomposed using the quantum Shannon decomposition (QSD) (Refs. [103, 123–125]). As

shown in Fig. 13, we need to implement the controlled $CU_{X_{8 \times 8}}$ as well as $CU_{X_{6 \times 6}}$ while minimizing non-Clifford gates. This can be done via ZX calculus [126] where we use pyzx [127]. For $CU_{X_{8 \times 8}}$, we obtain 156 R_Z and 301 Clifford gates. On the other hand, we have 158 R_Z and 215 Clifford gates for $CU_{X_{6 \times 6}}$. Finally, Fig. 14 shows the qubit decomposition of the circuit in Fig 13. To obtain the final qubit gate cost of this circuit, it remains to decompose the two $C\rho_{3^{(0)}}(X)^T$ and $C\rho_{3^{(0),*}}(X)^T$. These four controlled gates reduce to only two controlled gates with the use of two ancillas and four CCNOT gates resulting in a total cost for $C\rho_{3^{(0)}}(X)^T$ and $C\rho_{3^{(0),*}}(X)^T$ of 53 R_Z gates, 4 CCNOT and 2 ancillas.

Having constructed the Fourier gate, one need only implement a set of rotations along the diagonal of the transformed register, with angles given by the eigenvalues of the electric field Hamiltonian rescaled by trotter step and couplings. The eigenvalues can be found in Table IV.

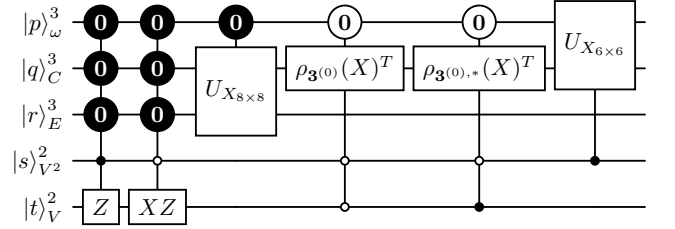


FIG. 13. Qutrit-qubit implementation of \mathfrak{D}_X for $\Sigma(72 \times 3)$.

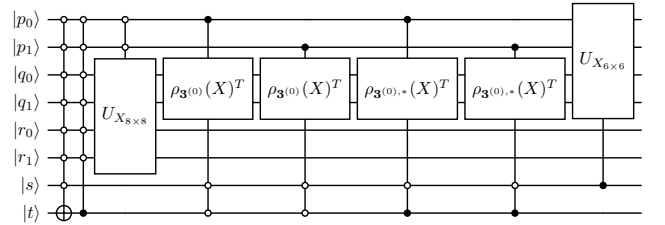


FIG. 14. Qubit implementation of \mathfrak{D}_X for $\Sigma(72 \times 3)$.

TABLE IV. Eigenvalues of the $\Sigma(72 \times 3)$ electric field Hamiltonian normalized by $g^2/2$. We combine certain irreps which have the same eigenvalue by denoting algebraic superscript a taking the values $1 \leq a \leq 3$.

ρ	$\mathbf{1}^{(0)}$	$\mathbf{1}^{(a)}$	$\mathbf{2}^{(0)}$	$\mathbf{3}^{(0)}$	$\mathbf{3}^{(a)}$	$\mathbf{3}^{(0),*}$	$\mathbf{3}^{(a),*}$	$\mathbf{6}^{(0)}$	$\mathbf{6}^{(1)}$	$\mathbf{8}$
$f(\rho)$	0	72	54	36	60	36	60	54	54	54

IX. RESOURCE COSTS

In order to estimate the fault-tolerant cost of our digitization, we use the following conversions. The Toffoli

TABLE V. T gate counts and clean ancilla required to implement gates from [111]

Gate	T gates	Clean ancilla
C ² NOT	7	0
C ³ NOT	21	1
C ⁴ NOT	35	2
CSWAP	7	0
R_Z	$1.15 \log_2(1/\epsilon)$	0
\mathfrak{U}_{-1}	637	4
\mathfrak{U}_\times	1120	5
\mathfrak{U}_{Tr}	$1414 + 8.05 \log_2(1/\epsilon)$	12
\mathfrak{U}_{FT}	$186295.4 \log_2(1/\epsilon) + 112$	5
\mathfrak{U}_ϕ	$294.4 \log_2(1/\epsilon)$	0

gate requires 7 T gates [111] and CⁿNOT gates can be constructed from $4(n-1)$ Toffoli gates and $n-1$ clean, reusable ancilla qubits¹ [111, 112]. We arrive at the cost for the R_Z gates via [128] where these gates can be approximated to precision ϵ with on average $1.15 \log(1/\epsilon)$ T gates [128]. Additionally, R_Y and R_X can be replaced by at most 1 R_Z gate and 2 Clifford transformations. Using these, we can construct fault-tolerant estimates assuming the T gate dominates, although this assumption has become questionable [129]. The number of T gates necessary to implement the various basic and primitive gates can be found in Tab. V.

One can consider combining these results with those of existing discrete subgroup primitives to estimate the scaling of these gates with $|G|$. A mild obstacle to this is we have only determined \mathfrak{U}_{FT} for $\Sigma(72 \times 3)$ rather than the more efficient \mathfrak{U}_{FFT} which are known for the other groups. To remedy this, we attempt the following estimate for a lower bound on the cost of $\mathfrak{U}_{FFT}^{\Sigma(72 \times 3)}$: replace the $\mathfrak{U}_{FT}^{\Sigma(36 \times 3)}$ used in $\mathfrak{U}_{FT}^{\Sigma(72 \times 3)}$ by the known $\mathfrak{U}_{FFT}^{\Sigma(36 \times 3)}$. Under this assumption, the cost for $\mathfrak{U}_{FFT}^{\Sigma(72 \times 3)}$ is estimated to be $515.2 \log_2(1/\epsilon) + 532$ T-gates, a 3 order of magnitude reduction compared to the \mathfrak{U}_{FT} . This is a strict lower bound on the cost of $\mathfrak{U}_{FFT}^{\Sigma(72 \times 3)}$ since this replacement can always be done at the cost of a more complex \mathfrak{D}_X . In Fig. 15, we compare the T-gate cost estimates for each primitive gate at a fixed error of $\epsilon = 10^{-10}$ for $\Sigma(72 \times 3)$ to $\mathbb{B}\mathbb{T}$, $\mathbb{B}\mathbb{O}$, $\Sigma(36 \times 3)$, and $\Sigma(72 \times 3)$. Across all groups, we find the ordering of costs is the same: \mathfrak{U}_{-1} , \mathfrak{U}_\times , \mathfrak{U}_{Tr} , \mathfrak{U}_{FFT} from cheapest to most expensive.

An interesting result is unlike $\mathbb{B}\mathbb{T}$ and $\Sigma(36 \times 3)$ where \mathfrak{U}_{Tr} requires $\sim 5 \times$ more T gates than \mathfrak{U}_\times , for $\mathbb{B}\mathbb{O}$ and $\Sigma(72 \times 3)$ the two gates has similar cost. It will be interesting to see if the remaining, larger groups $\mathbb{B}\mathbb{I}$, $\Sigma(216 \times 3)$, and $\Sigma(360 \times 3)$ keep this existing hierarchy. It is conceivable that for these groups that \mathfrak{U}_\times becomes more expen-

sive, since the number of trace classes grows sublinearly in $|G|$ despite fact that \mathfrak{U}_{Tr} requires R_Z synthesis.

Using our existing results, we can attempt to make extrapolations to predict the costs of remaining larger $SU(3)$ groups. One should be careful with this analysis since the $SU(2)$ and $SU(3)$ subgroups *do not* form a tower of groups. Thus prefactors in scaling relations may change between different $SU(N)$. Nevertheless using these results, we fit to two functional forms. The first is a linear logarithmic form for a “lower” bound:

$$f(|G|) = A + B|G| \log_2(|G|), \quad (40)$$

where $|G|$ is the size of the finite group $|G|$. We denote this fit form as polylog in the figure. The second is an “upper” bound that goes exponentially in group size:

$$h(|G|) = A + Be^{C|G|}. \quad (41)$$

The best fits for these forms are displayed alongside the known gate costs in Fig. 15 and Tab. VI contains the numerical predictions. These results suggest that the $\Sigma(216 \times 3)$ and $\Sigma(360 \times 3)$ gates will likely cost between $\sim 10 \times$ and $\sim 10^8 \times$ more T gates than $\Sigma(72 \times 3)$.

TABLE VI. Estimated number of T gates for $\Sigma(216 \times 3)$ and $\Sigma(360 \times 3)$.

Gate	$\Sigma(216 \times 3)$	$\Sigma(360 \times 3)$
\mathfrak{U}_{-1}	$10^3 - 10^6$	$10^3 - 10^9$
\mathfrak{U}_\times	$10^3 - 10^7$	$10^3 - 10^{12}$
\mathfrak{U}_{Tr}	$10^3 - 10^7$	$10^5 - 10^9$
\mathfrak{U}_{FFT}	$10^4 - 10^6$	$10^5 - 10^9$

Following [100, 130, 131], we integrate the primitive gates as subroutines into a quantum algorithm for computing the shear viscosity η on a $L^3 = 10^3$ lattice evolved for $N_t = 50$, and total synthesis error of $\epsilon_T = 10^{-8}$. We are neglecting state preparation (which can be substantial [70, 132–146]). We consider a Trotterized time evolution with step size δ and two Hamiltonians: the Kogut-Susskind H_{KS} [147] and the Symanzik-improved H_I [90]. For each of these, the number of primitive gates required per link per δt are listed in Tab. VII.

TABLE VII. Number of primitive gates per link per δt neglecting boundary effects as a function of d for H_{KS} and H_I .

Gate	$N[H_{KS}]$	$N[H_I]$
\mathfrak{U}_F	2	4
\mathfrak{U}_{Tr}	$\frac{1}{2}(d-1)$	$\frac{3}{2}(d-1)$
\mathfrak{U}_{-1}	$3(d-1)$	$2 + 11(d-1)$
\mathfrak{U}_\times	$6(d-1)$	$4 + 26(d-1)$

These results determine the total T gate count $N_T^H = C_T^H \times dL^d N_t$ for a d spatial lattice simulated for a time $t = N_t \delta t$. We find that for H_{KS} ,

$$C_T^{KS} = 9338d - 9114 + (372881 + 4.025d) \log_2 \frac{1}{\epsilon}. \quad (42)$$

¹ A *clean* ancilla is a qubit initialized to $|0\rangle$. *Dirty* ancilla indicate ones in an unknown initial state.

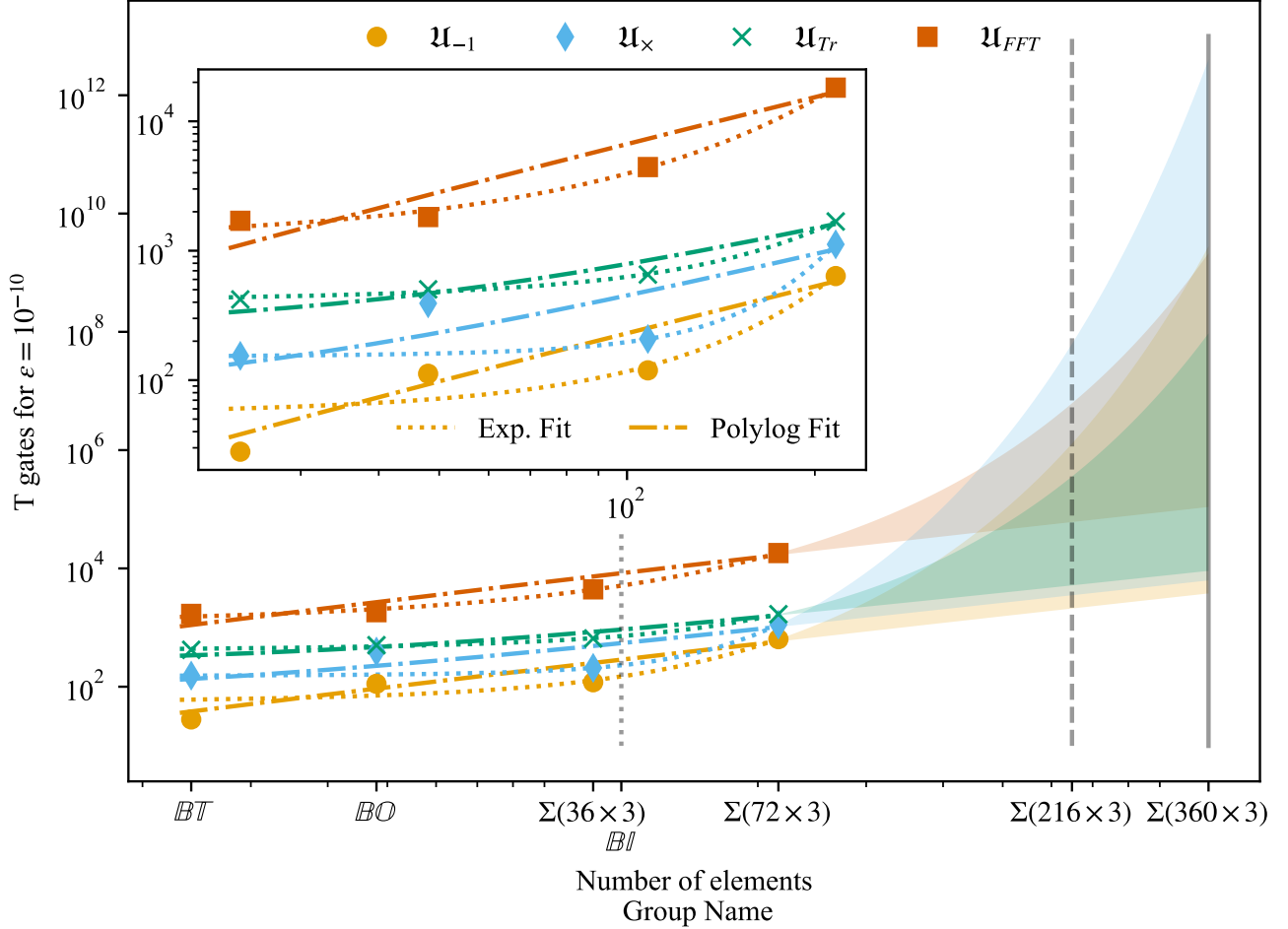


FIG. 15. T gate costs for the primitive gates \mathcal{U}_{-1} , \mathcal{U}_x , \mathcal{U}_{Tr} , and \mathcal{U}_{FFT} for the fixed synthesis precision $\epsilon = 10^{-10}$. Two extrapolations are shown: exponential and linear-logarithmic functional.

We estimate that the total synthesis error ϵ_T is the sum of ϵ from each R_Z . In the case of H_{KS} this yields

$$\epsilon_T = \frac{1}{2}(648489 + 7d)dL^d N_t \times \epsilon. \quad (43)$$

For H_I , the costs increase to

$$C_T^I = 38248d - 32046 + (745758 + 12.075d) \log_2 \frac{1}{\epsilon}, \quad (44)$$

where the total synthesis error is

$$\epsilon_T = \frac{1}{2}(1296971 + 21d)dL^d N_t \times \epsilon. \quad (45)$$

Kan and Nam estimated 6.5×10^{48} T gates would be required for an pure-gauge $SU(3)$ simulation of H_{KS} . This estimate used a truncated electric-field digitization and considerable fixed-point arithmetic. Here, using $\Sigma(72 \times 3)$ to approximate $SU(3)$ requires 7.1×10^{12} T gates for H_I and 3.5×10^{12} T gates for H_{KS} . The T gate density is roughly 1 per $\Sigma(72 \times 3)$ –register per clock cycle. Thus

$\Sigma(72 \times 3)$ reduces the gate costs of [131] by 10^{35} . Comparing to other discrete subgroups, these costs are nearly identical to those for the smaller $\Sigma(36 \times 3)$ without a fast Fourier transform [103], but 700 times more expensive than $\Sigma(36 \times 3)$ with the fast Fourier transform [119]. Similar to the previous results for discrete subgroups of $SU(N)$, without a full fast Fourier transform, \mathcal{U}_F dominates the simulations – being over 99% of the computation regardless of Hamiltonian.

While prior comparisons have been carried out with respect to Kan and Nam [131], more recent results have been proposed by Rhodes et al. [148] which utilizes block encodings of lattice gauge theories to help accelerate the quantum computation. Using a pure gauge calculation for various ranges of coefficients at the fixed volumes we consider yields roughly $10^{11} - 10^{14}$ T gates. For this reason we consider our results to be competitive with Ref. [148]. It may also prove that the large degree of sparsity present in discrete group approximation gate would yield a moderate improvement in computational costs compared to Trotterization however the systematic uncertainties

and renormalization effects would still remain an open question of research although there has been important recent progress [149].

X. OUTLOOK

In this work, we provided a construction of the quantum primitive gates to simulate the gauge degrees of freedom of $\Sigma(72 \times 3)$. This enables simulations of $SU(3)$ with higher levels of approximation than previous results based on $\Sigma(36 \times 3)$. The estimated T-gate cost incurred in computing the shear viscosity using these groups is found to be 7.1×10^{12} , a 35 orders of magnitude smaller than the T-gate cost estimated in Ref. [131]. Moreover, this cost is on par with [148]. Compared to $\Sigma(36 \times 3)$ (where a fast Fourier transform exists), the reduction in digitization error requires increasing the T gates cost by $700\times$.

With these results, the remaining crystal-like subgroups of $SU(3)$ are the two largest – $\Sigma(216 \times 3)$ and $\Sigma(360 \times 3)$ – which would further reduce digitization errors at the cost of a circuit depth. Using the scaling observed for previous crystal-like groups, we estimate $\Sigma(216 \times 3)$ may require 10^{13} to 10^{17} T-gates while $\Sigma(360 \times 3)$ would require between 10^{13} to 10^{20} . These costs would be substantially lower than estimated based on explicit constructions.

As we look ahead to the completion of the bosonic primitive gates for crystal-like subgroups, the next step is incorporating fermion fields [74, 150, 151]. Many methods exist to incorporate staggered and Wilson fermions while other fermion discretizations based on Ginsparg-Wilson relations require theoretical developments [152, 153]. It will be valuable to compare the resource costs for using different fermions not only in terms of T-gates but also using other methods such as [154].

ACKNOWLEDGMENTS

EG, EM and HL were supported by the U.S. Department of Energy, Office of Science, National Quantum Information Science Research Centers, Superconducting Quantum Materials and Systems Center (SQMS) under contract number DE-AC02-07CH11359 where EG’s part is under the NASA-DOE interagency agreement SAA2-403602. SO, HL and EG were supported by the U.S. Department of Energy, Office of Science, Office of High Energy Physics Quantum Information Science Enabled Discovery (QuantISED) programs “Intersections of QIS and Theoretical Particle Physics” and “Toward Lattice QCD on Quantum Computers” with EG under award number DE-SC0025940. EG was supported by the NASA Academic Mission Services, Contract No. NNA16BD14C and the Intelligent Systems Research and Development-3 (ISRDS-3) Contract 80ARC020D0010. EG acknowledges support from Universities Space Research Association for final review and edits of draft. This work was produced

by Fermi Forward Discovery Group, LLC under Contract No. 89243024CSC000002 with the U.S. Department of Energy, Office of Science, Office of High Energy Physics.

Appendix A: Staircase decompositions

Here, we discuss several decompositions of the CCSUM and Toffoli gates. The staircase rule for the Toffoli gate can be directly extended to C^n SUM gates regardless of control qudit dimension. One can verify that the decompositions shown in Fig. 16 holds. Once can see that the first CCSUM in the figure takes the initialized zero ancilla qutrit to the state $|ab\rangle$. The next CCSUM uses the control state on the ancilla plus the $|c\rangle$ to shift the bottom most qutrit to the state $|d \oplus_3 abc\rangle$. The final CCSUM uncomputes the ancilla qutrit.

TABLE VIII. Toffoli and T gate counts for various CCSUM gates. The first column corresponds to the dimensions of the control qudit e.g. “2-3” indicates a qubit and a qutrit control.

Control	Toffoli gates	T-gates
2	2	14
3	4	28
2-2	4	28
2-3	8	56
3-3	12	84
2-2-2	6	42
3-3-2	16	112

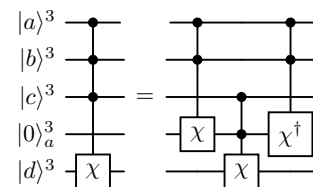


FIG. 16. Staircase decomposition of CCSUM into three CCSUM with one ancilla.

Other decompositions show how the C^n Sum gates are mapped to qubit. Given the qutrit CSUM has three possible outcomes ($\mathbb{1}_3$, χ , and χ^2), one has the circuit in Fig. 17 which applies the correct circuit in the “physical subspace.” The T-gate cost for the 4 Toffolis is 28. One can extend this to C^n Sum as shown in Fig. 17. In the special case of a C^n Sum controlled by both qubits and qutrits, we end up with a circuit that has fewer required Toffoli gates than in the case with two qutrit registers. Circuits for these and more complicated multicontrolled cases are provided in Fig. 17. We provided the T-gate costs and necessary ancilla for decomposing these heterogeneous circuits to homogeneous qubit circuits in Tab. VIII.

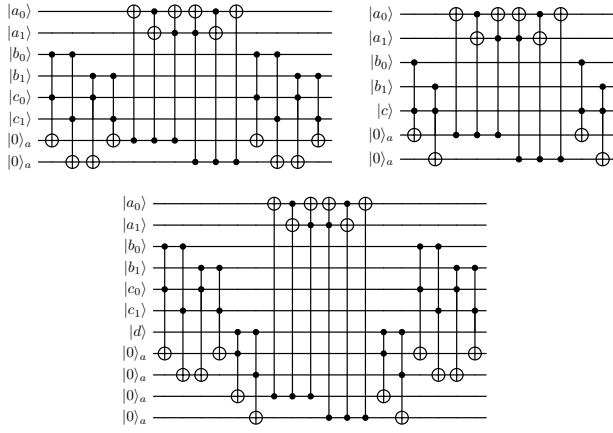


FIG. 17. Qubit decompositions of: (top left) a qutrit CCSUM, (top right) 2-3 CCSUM gate, (bottom) 2-3-3 CCCSUM gate.

-
- [1] G. Aarts, Introductory lectures on lattice qcd at nonzero baryon number, *Journal of Physics: Conference Series* **706**, 022004 (2016).
- [2] C. Gattringer and K. Langfeld, Approaches to the sign problem in lattice field theory, *Int. J. Mod. Phys. A* **31**, 1643007 (2016), arXiv:1603.09517 [hep-lat].
- [3] A. Alexandru, G. Basar, P. F. Bedaque, and N. C. Warrington, Complex paths around the sign problem, *Rev. Mod. Phys.* **94**, 015006 (2022), arXiv:2007.05436 [hep-lat].
- [4] M. Troyer and U.-J. Wiese, Computational complexity and fundamental limitations to fermionic quantum Monte Carlo simulations, *Phys. Rev. Lett.* **94**, 170201 (2005), arXiv:cond-mat/0408370 [cond-mat].
- [5] J. Unmuth-Yockey, J. Zhang, A. Bazavov, Y. Meurice, and S.-W. Tsai, Universal features of the Abelian Polyakov loop in 1+1 dimensions, *Phys. Rev. D* **98**, 094511 (2018), arXiv:1807.09186 [hep-lat].
- [6] J. F. Unmuth-Yockey, Gauge-invariant rotor Hamiltonian from dual variables of 3D $U(1)$ gauge theory, *Phys. Rev. D* **99**, 074502 (2019), arXiv:1811.05884 [hep-lat].
- [7] N. Klco, J. R. Stryker, and M. J. Savage, $SU(2)$ non-Abelian gauge field theory in one dimension on digital quantum computers, *Phys. Rev. D* **101**, 074512 (2020), arXiv:1908.06935 [quant-ph].
- [8] R. C. Farrell, M. Illa, A. N. Ciavarella, and M. J. Savage, Scalable Circuits for Preparing Ground States on Digital Quantum Computers: The Schwinger Model Vacuum on 100 Qubits, *PRX Quantum* **5**, 020315 (2024), arXiv:2308.04481 [quant-ph].
- [9] R. C. Farrell, M. Illa, A. N. Ciavarella, and M. J. Savage, Quantum simulations of hadron dynamics in the Schwinger model using 112 qubits, *Phys. Rev. D* **109**, 114510 (2024), arXiv:2401.08044 [quant-ph].
- [10] A. N. Ciavarella, String breaking in the heavy quark limit with scalable circuits, *Phys. Rev. D* **111**, 054501 (2025), arXiv:2411.05915 [quant-ph].
- [11] M. Illa, C. E. P. Robin, and M. J. Savage, Qu8its for quantum simulations of lattice quantum chromodynamics, *Phys. Rev. D* **110**, 014507 (2024), arXiv:2403.14537 [quant-ph].
- [12] A. Ciavarella, N. Klco, and M. J. Savage, Trailhead for quantum simulation of $SU(3)$ Yang-Mills lattice gauge theory in the local multiplet basis, *Phys. Rev. D* **103**, 094501 (2021), arXiv:2101.10227 [quant-ph].
- [13] A. Bazavov, Y. Meurice, S.-W. Tsai, J. Unmuth-Yockey, and J. Zhang, Gauge-invariant implementation of the Abelian Higgs model on optical lattices, *Phys. Rev. D* **92**, 076003 (2015), arXiv:1503.08354 [hep-lat].
- [14] J. Zhang, J. Unmuth-Yockey, J. Zeiher, A. Bazavov, S. W. Tsai, and Y. Meurice, Quantum simulation of the universal features of the Polyakov loop, *Phys. Rev. Lett.* **121**, 223201 (2018), arXiv:1803.11166 [hep-lat].
- [15] A. Bazavov, S. Catterall, R. G. Jha, and J. Unmuth-Yockey, Tensor renormalization group study of the non-abelian higgs model in two dimensions, *Phys. Rev. D* **99**, 114507 (2019).
- [16] C. W. Bauer and D. M. Grabowska, Efficient representation for simulating $U(1)$ gauge theories on digital quantum computers at all values of the coupling, *Phys. Rev. D* **107**, L031503 (2023), arXiv:2111.08015 [hep-ph].
- [17] D. M. Grabowska, C. Kane, B. Nachman, and C. W. Bauer, Overcoming exponential scaling with system size in Trotter-Suzuki implementations of constrained Hamiltonians: 2+1 $U(1)$ lattice gauge theories (2022), arXiv:2208.03333 [quant-ph].
- [18] A. J. Buser, T. Bhattacharya, L. Cincio, and R. Gupta, State preparation and measurement in a quantum simulation of the $O(3)$ sigma model, *Phys. Rev. D* **102**, 114514 (2020), arXiv:2006.15746 [quant-ph].
- [19] T. Bhattacharya, A. J. Buser, S. Chandrasekharan, R. Gupta, and H. Singh, Qubit regularization of asymptotic freedom, *Phys. Rev. Lett.* **126**, 172001 (2021), arXiv:2012.02153 [hep-lat].
- [20] A. H. Z. Kavaki and R. Lewis, From square plaquettes to triamond lattices for $SU(2)$ gauge theory, *Commun. Phys.* **7**, 208 (2024), arXiv:2401.14570 [hep-lat].
- [21] G. Calajò, G. Magnifico, C. Edmunds, M. Ringbauer, S. Montangero, and P. Silvi, Digital Quantum Simulation of a (1+1)D $SU(2)$ Lattice Gauge Theory with Ion Qu-

- aits, *PRX Quantum* **5**, 040309 (2024), [arXiv:2402.07987 \[quant-ph\]](#).
- [22] E. M. Murairi, M. J. Cervia, H. Kumar, P. F. Bedaque, and A. Alexandru, How many quantum gates do gauge theories require? (2022), [arXiv:2208.11789 \[hep-lat\]](#).
- [23] E. Zohar, J. I. Cirac, and B. Reznik, Quantum Simulations of Lattice Gauge Theories using Ultracold Atoms in Optical Lattices, *Rept. Prog. Phys.* **79**, 014401 (2016), [arXiv:1503.02312 \[quant-ph\]](#).
- [24] E. Zohar, J. I. Cirac, and B. Reznik, Cold-Atom Quantum Simulator for SU(2) Yang-Mills Lattice Gauge Theory, *Phys. Rev. Lett.* **110**, 125304 (2013), [arXiv:1211.2241 \[quant-ph\]](#).
- [25] E. Zohar, J. I. Cirac, and B. Reznik, Simulating Compact Quantum Electrodynamics with ultracold atoms: Probing confinement and nonperturbative effects, *Phys. Rev. Lett.* **109**, 125302 (2012), [arXiv:1204.6574 \[quant-ph\]](#).
- [26] E. Zohar, J. I. Cirac, and B. Reznik, Quantum simulations of gauge theories with ultracold atoms: local gauge invariance from angular momentum conservation, *Phys. Rev.* **A88**, 023617 (2013), [arXiv:1303.5040 \[quant-ph\]](#).
- [27] T. V. Zache, D. González-Cuadra, and P. Zoller, Quantum and Classical Spin-Network Algorithms for q-Deformed Kogut-Susskind Gauge Theories, *Phys. Rev. Lett.* **131**, 171902 (2023), [arXiv:2304.02527 \[quant-ph\]](#).
- [28] T. V. Zache, D. González-Cuadra, and P. Zoller, Fermion-qudit quantum processors for simulating lattice gauge theories with matter, *Quantum* **7**, 1140 (2023), [arXiv:2303.08683 \[quant-ph\]](#).
- [29] Z. Davoudi, C.-C. Hsieh, and S. V. Kadam, Scattering wave packets of hadrons in gauge theories: Preparation on a quantum computer, *Quantum* **8**, 1520 (2024), [arXiv:2402.00840 \[quant-ph\]](#).
- [30] I. Raychowdhury and J. R. Stryker, Solving Gauss's Law on Digital Quantum Computers with Loop-String-Hadron Digitization, *Phys. Rev. Res.* **2**, 033039 (2020), [arXiv:1812.07554 \[hep-lat\]](#).
- [31] S. V. Kadam, *Theoretical Developments in Lattice Gauge Theory for Applications in Double-beta Decay Processes and Quantum Simulation*, Ph.D. thesis, Maryland U., College Park (2023), [arXiv:2312.00780 \[hep-lat\]](#).
- [32] Z. Davoudi, I. Raychowdhury, and A. Shaw, Search for Efficient Formulations for Hamiltonian Simulation of non-Abelian Lattice Gauge Theories (2020), [arXiv:2009.11802 \[hep-lat\]](#).
- [33] E. Mathew and I. Raychowdhury, Protecting local and global symmetries in simulating (1+1)D non-Abelian gauge theories, *Phys. Rev. D* **106**, 054510 (2022), [arXiv:2206.07444 \[hep-lat\]](#).
- [34] M. Kreshchuk, W. M. Kirby, G. Goldstein, H. Beauchemin, and P. J. Love, Quantum Simulation of Quantum Field Theory in the Light-Front Formulation (2020), [arXiv:2002.04016 \[quant-ph\]](#).
- [35] M. Kreshchuk, S. Jia, W. M. Kirby, G. Goldstein, J. P. Vary, and P. J. Love, Simulating Hadronic Physics on NISQ devices using Basis Light-Front Quantization (2020), [arXiv:2011.13443 \[quant-ph\]](#).
- [36] M. Kreshchuk, S. Jia, W. M. Kirby, G. Goldstein, J. P. Vary, and P. J. Love, Light-Front Field Theory on Current Quantum Computers (2020), [arXiv:2009.07885 \[quant-ph\]](#).
- [37] J. Liu and Y. Xin, Quantum simulation of quantum field theories as quantum chemistry (2020), [arXiv:2004.13234 \[hep-th\]](#).
- [38] M. Fromm, O. Philipsen, W. Unger, and C. Winterowd, Quantum Gate Sets for Lattice QCD in the strong coupling limit: $N_f = 1$ (2023), [arXiv:2308.03196 \[hep-lat\]](#).
- [39] A. N. Ciavarella and C. W. Bauer, Quantum Simulation of SU(3) Lattice Yang Mills Theory at Leading Order in Large N (2024), [arXiv:2402.10265 \[hep-ph\]](#).
- [40] A. Alexandru, P. F. Bedaque, A. Carosso, M. J. Cervia, E. M. Murairi, and A. Sheng, Fuzzy gauge theory for quantum computers, *Phys. Rev. D* **109**, 094502 (2024), [arXiv:2308.05253 \[hep-lat\]](#).
- [41] R. Brower, S. Chandrasekharan, and U. J. Wiese, QCD as a quantum link model, *Phys. Rev.* **D60**, 094502 (1999), [arXiv:hep-th/9704106 \[hep-th\]](#).
- [42] H. Singh, Qubit regularized O(N) nonlinear sigma models, *Phys. Rev. D* **105**, 114509 (2022), [arXiv:1911.12353 \[hep-lat\]](#).
- [43] H. Singh and S. Chandrasekharan, Qubit regularization of the O(3) sigma model, *Phys. Rev. D* **100**, 054505 (2019), [arXiv:1905.13204 \[hep-lat\]](#).
- [44] U.-J. Wiese, Towards Quantum Simulating QCD, *Proceedings, 24th International Conference on Ultra-Relativistic Nucleus-Nucleus Collisions (Quark Matter 2014): Darmstadt, Germany, May 19-24, 2014*, *Nucl. Phys.* **A931**, 246 (2014), [arXiv:1409.7414 \[hep-th\]](#).
- [45] R. C. Brower, D. Berenstein, and H. Kawai, Lattice Gauge Theory for a Quantum Computer, *PoS LAT-TICE2019*, 112 (2019), [arXiv:2002.10028 \[hep-lat\]](#).
- [46] S. V. Mathis, G. Mazzola, and I. Tavernelli, Toward scalable simulations of Lattice Gauge Theories on quantum computers, *Phys. Rev. D* **102**, 094501 (2020), [arXiv:2005.10271 \[quant-ph\]](#).
- [47] J. C. Halimeh, R. Ott, I. P. McCulloch, B. Yang, and P. Hauke, Robustness of gauge-invariant dynamics against defects in ultracold-atom gauge theories, *Phys. Rev. Res.* **2**, 033361 (2020), [arXiv:2005.10249 \[cond-mat.quant-gas\]](#).
- [48] T. Budde, M. Krstić Marinković, and J. C. P. Barros, Quantum many-body scars for arbitrary integer spin in 2+1D Abelian gauge theories (2024), [arXiv:2403.08892 \[hep-lat\]](#).
- [49] T. Budde, M. Krstić Marinković, and J. C. P. Barros, Quantum many-body scars for arbitrary integer spin in 2+1D Abelian gauge theories (2024), [arXiv:2403.08892 \[hep-lat\]](#).
- [50] J. Osborne, B. Yang, I. P. McCulloch, P. Hauke, and J. C. Halimeh, Spin-SU(1) Quantum Link Models with Dynamical Matter on a Quantum Simulator (2023), [arXiv:2305.06368 \[cond-mat.quant-gas\]](#).
- [51] D. Luo, J. Shen, M. Highman, B. K. Clark, B. DeMarco, A. X. El-Khadra, and B. Gadway, Framework for simulating gauge theories with dipolar spin systems, *Phys. Rev. A* **102**, 032617 (2020), [arXiv:1912.11488 \[quant-ph\]](#).
- [52] P. Orland and D. Rohrlich, Lattice gauge magnets: Local isospin from spin, *Nuclear Physics B* **338**, 647 (1990).
- [53] E. Gustafson *et al.*, Large scale multi-node simulations of \mathbb{Z}_2 gauge theory quantum circuits using Google Cloud Platform, in *IEEE/ACM Second International Workshop on Quantum Computing Software* (2021) [arXiv:2110.07482 \[quant-ph\]](#).
- [54] E. Gustafson, Prospects for Simulating a Qudit Based Model of (1+1)d Scalar QED, *Phys. Rev. D* **103**, 114505 (2021), [arXiv:2104.10136 \[quant-ph\]](#).
- [55] P. P. Popov, M. Meth, M. Lewenstein, P. Hauke, M. Ringbauer, E. Zohar, and V. Kasper, Variational quantum

- simulation of U(1) lattice gauge theories with qudit systems, *Phys. Rev. Res.* **6**, 013202 (2024).
- [56] D. M. Kurkcuoglu, M. S. Alam, J. A. Job, A. C. Y. Li, A. Macridin, G. N. Perdue, and S. Providence, Quantum simulation of ϕ^4 theories in qudit systems (2022), [arXiv:2108.13357 \[quant-ph\]](#).
- [57] D. González-Cuadra, T. V. Zache, J. Carrasco, B. Kraus, and P. Zoller, Hardware Efficient Quantum Simulation of Non-Abelian Gauge Theories with Qudits on Rydberg Platforms, *Phys. Rev. Lett.* **129**, 160501 (2022), [arXiv:2203.15541 \[quant-ph\]](#).
- [58] V. Ale, N. M. Bauer, R. G. Jha, F. Ringer, and G. Siopsis, Quantum computation of SU(2) lattice gauge theory with continuous variables, *JHEP* **06** (084), [arXiv:2410.14580 \[hep-lat\]](#).
- [59] G. Pardo, J. Bender, N. Katz, and E. Zohar, Truncation-free quantum simulation of pure-gauge compact QED using Josephson arrays, *Quantum Sci. Technol.* **10**, 035011 (2025), [arXiv:2410.11413 \[hep-lat\]](#).
- [60] J. Bender, E. Zohar, A. Farace, and J. I. Cirac, Digital quantum simulation of lattice gauge theories in three spatial dimensions, *New J. Phys.* **20**, 093001 (2018), [arXiv:1804.02082 \[quant-ph\]](#).
- [61] D. C. Hackett, K. Howe, C. Hughes, W. Jay, E. T. Neil, and J. N. Simone, Digitizing Gauge Fields: Lattice Monte Carlo Results for Future Quantum Computers, *Phys. Rev. A* **99**, 062341 (2019), [arXiv:1811.03629 \[quant-ph\]](#).
- [62] A. Alexandru, P. F. Bedaque, S. Harmalkar, H. Lamm, S. Lawrence, and N. C. Warrington (NuQS), Gluon field digitization for quantum computers, *Phys.Rev.D* **100**, 114501 (2019), [arXiv:1906.11213 \[hep-lat\]](#).
- [63] A. Yamamoto, Real-time simulation of (2+1)-dimensional lattice gauge theory on qubits, *PTEP* **2021**, 013B06 (2021), [arXiv:2008.11395 \[hep-lat\]](#).
- [64] Y. Ji, H. Lamm, and S. Zhu (NuQS), Gluon Field Digitization via Group Space Decimation for Quantum Computers, *Phys. Rev. D* **102**, 114513 (2020), [arXiv:2005.14221 \[hep-lat\]](#).
- [65] J. F. Haase, L. Dellantonio, A. Celi, D. Paulson, A. Kan, K. Jansen, and C. A. Muschik, A resource efficient approach for quantum and classical simulations of gauge theories in particle physics, *Quantum* **5**, 393 (2021), [arXiv:2006.14160 \[quant-ph\]](#).
- [66] M. Carena, H. Lamm, Y.-Y. Li, and W. Liu, Lattice Renormalization of Quantum Simulations (2021), [arXiv:2107.01166 \[hep-lat\]](#).
- [67] T. Armon, S. Ashkenazi, G. García-Moreno, A. González-Tudela, and E. Zohar, Photon-Mediated Stroboscopic Quantum Simulation of a Z2 Lattice Gauge Theory, *Phys. Rev. Lett.* **127**, 250501 (2021), [arXiv:2107.13024 \[quant-ph\]](#).
- [68] C. Charles, E. J. Gustafson, E. Hardt, F. Herren, N. Hogan, H. Lamm, S. Starecheski, R. S. Van de Water, and M. L. Wagman, Simulating Z2 lattice gauge theory on a quantum computer, *Phys. Rev. E* **109**, 015307 (2024), [arXiv:2305.02361 \[hep-lat\]](#).
- [69] R. Irmejs, M. C. Banuls, and J. I. Cirac, Quantum simulation of Z2 lattice gauge theory with minimal resources, *Phys. Rev. D* **108**, 074503 (2023).
- [70] E. J. Gustafson and H. Lamm, Toward quantum simulations of \mathbb{Z}_2 gauge theory without state preparation, *Phys. Rev. D* **103**, 054507 (2021), [arXiv:2011.11677 \[hep-lat\]](#).
- [71] T. Hartung, T. Jakobs, K. Jansen, J. Ostmeier, and C. Urbach, Digitising SU(2) gauge fields and the freezing transition, *Eur. Phys. J. C* **82**, 237 (2022), [arXiv:2201.09625 \[hep-lat\]](#).
- [72] M. Carena, H. Lamm, Y.-Y. Li, and W. Liu, Quantum error thresholds for gauge-redundant digitizations of lattice field theories, *Phys. Rev. D* **110**, 054516 (2024), [arXiv:2402.16780 \[hep-lat\]](#).
- [73] E. Zohar and M. Burrello, Formulation of lattice gauge theories for quantum simulations, *Phys. Rev. D* **91**, 054506 (2015), [arXiv:1409.3085 \[quant-ph\]](#).
- [74] E. Zohar, A. Farace, B. Reznik, and J. I. Cirac, Digital lattice gauge theories, *Phys. Rev. A* **95**, 023604 (2017), [arXiv:1607.08121 \[quant-ph\]](#).
- [75] N. Mueller, T. Wang, O. Katz, Z. Davoudi, and M. Cetina, Quantum computing universal thermalization dynamics in a (2 + 1)D Lattice Gauge Theory, *Nature Commun.* **16**, 5492 (2025), [arXiv:2408.00069 \[quant-ph\]](#).
- [76] M. Creutz, L. Jacobs, and C. Rebbi, Monte Carlo Study of Abelian Lattice Gauge Theories, *Phys. Rev. D* **20**, 1915 (1979).
- [77] M. Creutz and M. Okawa, Generalized Actions in $Z(p)$ Lattice Gauge Theory, *Nucl. Phys.* **B220**, 149 (1983).
- [78] G. Bhanot and C. Rebbi, Monte Carlo Simulations of Lattice Models With Finite Subgroups of SU(3) as Gauge Groups, *Phys. Rev. D* **24**, 3319 (1981).
- [79] D. Petcher and D. H. Weingarten, Monte Carlo Calculations and a Model of the Phase Structure for Gauge Theories on Discrete Subgroups of SU(2), *Phys. Rev. D* **22**, 2465 (1980).
- [80] G. Bhanot, SU(3) Lattice Gauge Theory in Four-dimensions With a Modified Wilson Action, *Phys. Lett.* **108B**, 337 (1982).
- [81] Y. Ji, H. Lamm, and S. Zhu (NuQS), Gluon digitization via character expansion for quantum computers, *Phys. Rev. D* **107**, 114503 (2023), [arXiv:2203.02330 \[hep-lat\]](#).
- [82] A. Alexandru, P. F. Bedaque, R. Brett, and H. Lamm, Spectrum of digitized QCD: Glueballs in a S(1080) gauge theory, *Phys. Rev. D* **105**, 114508 (2022), [arXiv:2112.08482 \[hep-lat\]](#).
- [83] M. Carena, E. J. Gustafson, H. Lamm, Y.-Y. Li, and W. Liu, Gauge theory couplings on anisotropic lattices, *Phys. Rev. D* **106**, 114504 (2022), [arXiv:2208.10417 \[hep-lat\]](#).
- [84] D. H. Weingarten and D. N. Petcher, Monte Carlo Integration for Lattice Gauge Theories with Fermions, *Phys. Lett.* **99B**, 333 (1981).
- [85] D. Weingarten, Monte Carlo Evaluation of Hadron Masses in Lattice Gauge Theories with Fermions, *Phys. Lett.* **109B**, 57 (1982), [631(1981)].
- [86] A. Rajput, A. Roggero, and N. Wiebe, Quantum error correction with gauge symmetries (2023), [arXiv:2112.05186 \[quant-ph\]](#).
- [87] L. Spagnoli, A. Roggero, and N. Wiebe, Fault-tolerant simulation of Lattice Gauge Theories with gauge covariant codes (2024), [arXiv:2405.19293 \[quant-ph\]](#).
- [88] D. M. Kürkçüoğlu, H. Lamm, O. Ogunkoya, and L. Pierattelli, The 2T-quocit: a two-mode bosonic qudit for high energy physics (2025), [arXiv:2509.21941 \[quant-ph\]](#).
- [89] J. Haruna, Note on Logical Gates by Gauge Field Formalism of Quantum Error Correction (2025), [arXiv:2511.15224 \[hep-th\]](#).
- [90] M. Carena, H. Lamm, Y.-Y. Li, and W. Liu, Improved Hamiltonians for Quantum Simulations of Gauge Theories, *Phys. Rev. Lett.* **129**, 051601 (2022),

- arXiv:2203.02823 [hep-lat].
- [91] B. Assi and H. Lamm, Digitization and subduction of $SU(N)$ gauge theories, *Phys. Rev. D* **110**, 074511 (2024), arXiv:2405.12204 [hep-lat].
- [92] J. B. Kogut, $1/n$ Expansions and the Phase Diagram of Discrete Lattice Gauge Theories With Matter Fields, *Phys. Rev. D* **21**, 2316 (1980).
- [93] J. Romers, *Discrete gauge theories in two spatial dimensions*, Ph.D. thesis, Master's thesis, Universiteit van Amsterdam (2007).
- [94] E. H. Fradkin and S. H. Shenker, Phase Diagrams of Lattice Gauge Theories with Higgs Fields, *Phys. Rev. D* **19**, 3682 (1979).
- [95] D. Harlow and H. Ooguri, Symmetries in quantum field theory and quantum gravity, *Commun. Math. Phys.* **383**, 1669 (2021), arXiv:1810.05338 [hep-th].
- [96] D. Horn, M. Weinstein, and S. Yankielowicz, Hamiltonian Approach to $Z(N)$ Lattice Gauge Theories, *Phys. Rev. D* **19**, 3715 (1979).
- [97] H. Lamm, S. Lawrence, and Y. Yamauchi (NuQS), General Methods for Digital Quantum Simulation of Gauge Theories, *Phys. Rev. D* **100**, 034518 (2019), arXiv:1903.08807 [hep-lat].
- [98] M. S. Alam, S. Hadfield, H. Lamm, and A. C. Y. Li (SQMS), Primitive quantum gates for dihedral gauge theories, *Phys. Rev. D* **105**, 114501 (2022), arXiv:2108.13305 [quant-ph].
- [99] M. Fromm, O. Philipsen, and C. Winterowd, Dihedral lattice gauge theories on a quantum annealer, *EPJ Quant. Technol.* **10**, 31 (2023), arXiv:2206.14679 [hep-lat].
- [100] E. J. Gustafson, H. Lamm, F. Lovelace, and D. Musk, Primitive quantum gates for an $SU(2)$ discrete subgroup: Binary tetrahedral, *Phys. Rev. D* **106**, 114501 (2022), arXiv:2208.12309 [quant-ph].
- [101] E. J. Gustafson, H. Lamm, and F. Lovelace, Primitive quantum gates for an $SU(2)$ discrete subgroup: Binary octahedral, *Phys. Rev. D* **109**, 054503 (2024), arXiv:2312.10285 [hep-lat].
- [102] H. Lamm, Y.-Y. Li, J. Shu, Y.-L. Wang, and B. Xu, Block encodings of discrete subgroups on a quantum computer, *Phys. Rev. D* **110**, 054505 (2024), arXiv:2405.12890 [hep-lat].
- [103] E. J. Gustafson, Y. Ji, H. Lamm, E. M. Muraïri, S. O. Perez, and S. Zhu, Primitive quantum gates for an $SU(3)$ discrete subgroup: $\Sigma(36 \times 3)$, *Phys. Rev. D* **110**, 034515 (2024), arXiv:2405.05973 [hep-lat].
- [104] G. Clemente, A. Crippa, and K. Jansen, Strategies for the determination of the running coupling of $(2+1)$ -dimensional QED with quantum computing, *Phys. Rev. D* **106**, 114511 (2022), arXiv:2206.12454 [hep-lat].
- [105] L. Funcke, C. F. Groß, K. Jansen, S. Kühn, S. Romiti, and C. Urbach, Hamiltonian limit of lattice QED in $2+1$ dimensions, *PoS LATTICE2022*, 292 (2023), arXiv:2212.09627 [hep-lat].
- [106] A. Crippa, S. Romiti, L. Funcke, K. Jansen, S. Kühn, P. Stornati, and C. Urbach, Towards determining the $(2+1)$ -dimensional Quantum Electrodynamics running coupling with Monte Carlo and quantum computing methods (2024), arXiv:2404.17545 [hep-lat].
- [107] W. Grimus and P. O. Ludl, Principal series of finite subgroups of $SU(3)$, *J. Phys. A* **43**, 445209 (2010), arXiv:1006.0098 [hep-ph].
- [108] E. J. Gustafson and H. Lamm, Robustness of Gauge Digitization to Quantum Noise (2023), arXiv:2301.10207 [hep-lat].
- [109] Y.-M. Di and H.-R. Wei, Elementary gates for ternary quantum logic circuit (2011), arXiv:1105.5485 [quant-ph].
- [110] J. M. Baker, C. Duckering, A. Hoover, and F. T. Chong, Decomposing Quantum Generalized Toffoli with an Arbitrary Number of Ancilla (2019), arXiv:1904.01671 [quant-ph].
- [111] I. L. Chuang and M. A. Nielsen, Prescription for experimental determination of the dynamics of a quantum black box, *J. Mod. Opt.* **44**, 2455 (1997), arXiv:quant-ph/9610001.
- [112] A. Barenco, C. H. Bennett, R. Cleve, D. P. DiVincenzo, N. Margolus, P. Shor, T. Sleator, J. A. Smolin, and H. Weinfurter, Elementary gates for quantum computation, *Phys. Rev. A* **52**, 3457 (1995).
- [113] A. Y. Kitaev, *Quantum measurements and the Abelian stabilizer problem* (1995), arXiv:quant-ph/9511026.
- [114] M. A. Nielsen and I. Chuang, *Quantum computation and quantum information* (Cambridge University Press, 2002).
- [115] L. Hales and S. Hallgren, An improved quantum fourier transform algorithm and applications, in *Proceedings 41st Annual Symposium on Foundations of Computer Science* (IEEE, 2000) pp. 515–525.
- [116] P. Hoyer, Efficient quantum transforms (1997), arXiv:quant-ph/9702028.
- [117] R. Beals, Quantum computation of fourier transforms over symmetric groups, in *Proceedings of the twenty-ninth annual ACM symposium on Theory of computing* (1997) pp. 48–53.
- [118] M. Püschel, M. Rötteler, and T. Beth, Fast quantum Fourier transforms for a class of non-abelian groups, in *Applied Algebra, Algebraic Algorithms and Error-Correcting Codes: 13th International Symposium, AAEECC-13 Honolulu, Hawaii, USA, November 15–19, 1999 Proceedings 13* (Springer, 1999) pp. 148–159.
- [119] E. M. Muraïri, M. Sohaib Alam, H. Lamm, S. Hadfield, and E. Gustafson, Highly-efficient quantum Fourier transformations for certain non-Abelian groups, *Phys. Rev. D* **110**, 074501 (2024), arXiv:2408.00075 [quant-ph].
- [120] C. Moore, D. Rockmore, and A. Russell, Generic quantum Fourier transforms, *ACM Transactions on Algorithms (TALG)* **2**, 707 (2006).
- [121] A. Mariani, S. Pradhan, and E. Ercolessi, Hamiltonians and gauge-invariant hilbert space for lattice yang-mills-like theories with finite gauge group, *Phys. Rev. D* **107**, 114513 (2023).
- [122] M. Püschel, M. Rötteler, and T. Beth, Fast quantum fourier transforms for a class of non-abelian groups, in *Applied Algebra, Algebraic Algorithms and Error-Correcting Codes*, edited by M. Fossorier, H. Imai, S. Lin, and A. Poli (Springer Berlin Heidelberg, Berlin, Heidelberg, 1999) pp. 148–159.
- [123] C. Paige and M. Wei, History and generality of the cs decomposition, *Linear Algebra and its Applications* **208-209**, 303 (1994).
- [124] Y. Chen and J. Wang, Qcompiler: Quantum compilation with the csd method, *Computer Physics Communications* **184**, 853 (2013).
- [125] Y.-M. Di and H.-R. Wei, Optimal synthesis of multivalued quantum circuits, *Phys. Rev. A* **92**, 062317 (2015).
- [126] R. Duncan, A. Kissinger, S. Perdrix, and J. van de Wetering, Graph-theoretic Simplification of Quantum

- Circuits with the ZX-calculus, *Quantum* **4**, 279 (2020).
- [127] A. Kissinger and J. van de Wetering, PyZX: Large Scale Automated Diagrammatic Reasoning, in *Proceedings 16th International Conference on Quantum Physics and Logic*, Chapman University, Orange, CA, USA., 10-14 June 2019, Electronic Proceedings in Theoretical Computer Science, Vol. 318, edited by B. Coecke and M. Leifer (Open Publishing Association, 2020) pp. 229–241.
- [128] A. Bocharov, M. Roetteler, and K. M. Svore, Efficient synthesis of universal repeat-until-success quantum circuits, *Phys. Rev. Lett.* **114**, 080502 (2015).
- [129] C. Gidney, N. Shutty, and C. Jones, Magic state cultivation: growing T states as cheap as CNOT gates (2024), [arXiv:2409.17595](https://arxiv.org/abs/2409.17595) [quant-ph].
- [130] T. D. Cohen, H. Lamm, S. Lawrence, and Y. Yamauchi (NuQS), Quantum algorithms for transport coefficients in gauge theories, *Phys. Rev. D* **104**, 094514 (2021), [arXiv:2104.02024](https://arxiv.org/abs/2104.02024) [hep-lat].
- [131] A. Kan and Y. Nam, Lattice Quantum Chromodynamics and Electrodynamics on a Universal Quantum Computer (2021), [arXiv:2107.12769](https://arxiv.org/abs/2107.12769) [quant-ph].
- [132] X.-D. Xie, X. Guo, H. Xing, Z.-Y. Xue, D.-B. Zhang, and S.-L. Zhu (QuNu), Variational thermal quantum simulation of the lattice Schwinger model, *Phys. Rev. D* **106**, 054509 (2022), [arXiv:2205.12767](https://arxiv.org/abs/2205.12767) [quant-ph].
- [133] Z. Davoudi, N. Mueller, and C. Powers, Towards Quantum Computing Phase Diagrams of Gauge Theories with Thermal Pure Quantum States, *Phys. Rev. Lett.* **131**, 081901 (2023), [arXiv:2208.13112](https://arxiv.org/abs/2208.13112) [hep-lat].
- [134] A. Avkhadiev, P. E. Shanahan, and R. D. Young, Accelerating Lattice Quantum Field Theory Calculations via Interpolator Optimization Using Noisy Intermediate-Scale Quantum Computing, *Phys. Rev. Lett.* **124**, 080501 (2020), [arXiv:1908.04194](https://arxiv.org/abs/1908.04194) [hep-lat].
- [135] E. J. Gustafson, Stout Smearing on a Quantum Computer (2022), [arXiv:2211.05607](https://arxiv.org/abs/2211.05607) [hep-lat].
- [136] A. Peruzzo, J. McClean, P. Shadbolt, M.-H. Yung, X.-Q. Zhou, P. J. Love, A. Aspuru-Guzik, and J. L. O’Brien, A variational eigenvalue solver on a photonic quantum processor, *Nature communications* **5**, 4213 (2014).
- [137] E. Gustafson, Y. Meurice, and J. Unmuth-Yockey, Quantum simulation of scattering in the quantum Ising model, *Phys. Rev. D* **99**, 094503 (2019), [arXiv:1901.05944](https://arxiv.org/abs/1901.05944) [hep-lat].
- [138] E. Gustafson, P. Dreher, Z. Hang, and Y. Meurice, Benchmarking quantum computers for real-time evolution of a $(1+1)$ field theory with error mitigation, *Quantum Sci. Technol.* **6**, 045020 (2021), [arXiv:1910.09478](https://arxiv.org/abs/1910.09478) [hep-lat].
- [139] S. Harmalkar, H. Lamm, and S. Lawrence (NuQS), Quantum Simulation of Field Theories Without State Preparation (2020), [arXiv:2001.11490](https://arxiv.org/abs/2001.11490) [hep-lat].
- [140] S. P. Jordan, H. Krovi, K. S. Lee, and J. Preskill, BQP-completeness of Scattering in Scalar Quantum Field Theory, *Quantum* **2**, 44 (2018), [arXiv:1703.00454](https://arxiv.org/abs/1703.00454) [quant-ph].
- [141] A. Riera, C. Gogolin, and J. Eisert, Thermalization in nature and on a quantum computer, *Phys. Rev. Lett.* **108**, 080402 (2012).
- [142] M. Motta, C. Sun, A. T. Tan, M. J. O’Rourke, E. Ye, A. J. Minnich, F. G. Brandao, and G. K.-L. Chan, Determining eigenstates and thermal states on a quantum computer using quantum imaginary time evolution, *Nature Physics* **16**, 205 (2020).
- [143] G. Clemente *et al.* (QuBiPF), Quantum computation of thermal averages in the presence of a sign problem, *Phys. Rev. D* **101**, 074510 (2020), [arXiv:2001.05328](https://arxiv.org/abs/2001.05328) [hep-lat].
- [144] W. A. de Jong, K. Lee, J. Mulligan, M. Płoskoń, F. Ringer, and X. Yao, Quantum simulation of nonequilibrium dynamics and thermalization in the Schwinger model, *Phys. Rev. D* **106**, 054508 (2022), [arXiv:2106.08394](https://arxiv.org/abs/2106.08394) [quant-ph].
- [145] E. J. Gustafson, H. Lamm, and J. Unmuth-Yockey, Quantum mean estimation for lattice field theory, *Phys. Rev. D* **107**, 114511 (2023), [arXiv:2303.00094](https://arxiv.org/abs/2303.00094) [hep-lat].
- [146] C. F. Kane, N. Gomes, and M. Kreshchuk, Nearly optimal state preparation for quantum simulations of lattice gauge theories, *Phys. Rev. A* **110**, 012455 (2024), [arXiv:2310.13757](https://arxiv.org/abs/2310.13757) [quant-ph].
- [147] J. Kogut and L. Susskind, Hamiltonian formulation of Wilson’s lattice gauge theories, *Phys. Rev. D* **11**, 395 (1975).
- [148] M. L. Rhodes, M. Kreshchuk, and S. Pathak, Exponential Improvements in the Simulation of Lattice Gauge Theories Using Near-Optimal Techniques, *PRX Quantum* **5**, 040347 (2024), [arXiv:2405.10416](https://arxiv.org/abs/2405.10416) [quant-ph].
- [149] C. F. Kane, S. Hariprakash, and C. W. Bauer, Obtaining continuum physics from dynamical simulations of Hamiltonian lattice gauge theories (2025), [arXiv:2506.16559](https://arxiv.org/abs/2506.16559) [hep-lat].
- [150] A. Florio, A. Weichselbaum, S. Valgushev, and R. D. Pisarski, Mass gaps of a Z3 gauge theory with three fermion flavors in 1+1 dimensions, *Phys. Rev. D* **110**, 045013 (2024), [arXiv:2310.18312](https://arxiv.org/abs/2310.18312) [hep-th].
- [151] P. Emonts and E. Zohar, Gauss law, Minimal Coupling and Fermionic PEPS for Lattice Gauge Theories, in *Tensor Network and entanglement* (2018) [arXiv:1807.01294](https://arxiv.org/abs/1807.01294) [quant-ph].
- [152] M. Clancy, Toward a Ginsparg-Wilson lattice Hamiltonian, *Phys. Rev. D* **110**, L011502 (2024), [arXiv:2312.08647](https://arxiv.org/abs/2312.08647) [hep-lat].
- [153] H. Singh, Ginsparg-Wilson Hamiltonians with Improved Chiral Symmetry (2025), [arXiv:2505.20419](https://arxiv.org/abs/2505.20419) [hep-lat].
- [154] K. Gui, A. M. Dalzell, A. Achille, M. Suchara, and F. T. Chong, Spacetime-Efficient Low-Depth Quantum State Preparation with Applications, *Quantum* **8**, 1257 (2024), [arXiv:2303.02131](https://arxiv.org/abs/2303.02131) [quant-ph].